



City Research Online

City St George's, University of London

Citation: Wang, Z., Rajana, K., Corfar, D. & Tsavdaridis, K. D. (2023). Automated Minimum-Weight Sizing Design Routine for Tall Self-Standing Modular Buildings Subjected to Multiple Performance Constraints Under Static and Dynamic Wind Loads. *Engineering Structures*, 286, 116121. doi: 10.1016/j.engstruct.2023.116121

This is the published version of the paper.

This version of the publication may differ from the final published version. To cite this item please consult the publisher's version.

Permanent repository link: <https://openaccess.city.ac.uk/id/eprint/30219/>

Link to published version: <https://doi.org/10.1016/j.engstruct.2023.116121>

Copyright and Reuse: Copyright and Moral Rights remain with the author(s) and/or copyright holders. Copies of full items can be used for personal research or study, educational, or not-for-profit purposes without prior permission or charge, unless otherwise indicated, provided that the authors, title and full bibliographic details are credited, a hyperlink and/or URL is given for the original metadata page and the content is not changed in any way. For full details of reuse please refer to [City Research Online policy](#).



Automated minimum-weight sizing design framework for tall self-standing modular buildings subjected to multiple performance constraints under static and dynamic wind loads

Zixiao Wang^a, Komal Rajana^a, Dan-Adrian Corfar^a, Konstantinos Daniel Tsavdaridis^{a,*}

^a Department of Engineering, School of Science & Technology, City, University of London, UK

ARTICLE INFO

Keywords:

Structural sizing optimisation
Modular building systems
Wind effects
SAP2000 Open Application Programming Interface

ABSTRACT

In recent decades, the shortage of affordable housing has become an endemic issue in many cities worldwide due to the ongoing urban population growth. Against this backdrop, volumetric steel modular building systems (MBSs) are becoming an increasingly compelling solution to the above challenge owing to their rapid construction speed and reduced upfront costs. Notwithstanding their success in low- to mid-rise projects, these assembled structures generally rely on a separate lateral load-resisting system (LLRS) for lateral stiffness and resistance to increased wind loads as the building altitude increases. However, additional LLRSs require on-site construction, thereby compromising the productivity boost offered by the MBSs. To this end, this paper proposes a novel optimisation-driven sizing design framework for tall self-standing modular buildings subjected to concurrent drift, floor acceleration, and member strength constraints under static and dynamic wind loads. A computationally efficient solution strategy is devised to facilitate a meaningful sizing solution by decomposing the constrained discrete sizing problem into a convex serviceability limit stage (SLS) and a non-convex ultimate limit stage (ULS), which can be then solved using preferred local and global optimisation methods, separately. The framework is implemented by integrating SAP2000 (for structural analysis) and MATLAB (for optimisation) through SAP2000's open Application Programming Interface (API), and demonstrated using a 15-storey self-standing steel modular building exposed to three different levels of wind intensity. A comprehensive performance assessment is conducted on the optimally designed case-study building to investigate its elastic instability behaviour, geometric nonlinear effects on wind-induced response, and impacts of global sway imperfections on member utilisation ratios under wind effects. It is concluded that tall self-standing modular buildings can be achieved economically using ordinary corner-supported modules without ad hoc structural provisions, while consuming steel at similar rates to conventional building structural systems. Furthermore, the proposed sizing framework and solution strategy have proven to be useful design tools for reconciling the structural resilience and material efficiency in wind-sensitive self-standing modular buildings.

1. Introduction

In recent decades, global population growth and rapid urbanisation trends have created endemic housing shortages and sharp upturns in compact high-rise developments in many major cities worldwide. With the projection that 68% of the world's population will live in urban areas by 2050 [1], a partial solution to the growing pressure on urban housing is to build more affordable homes at a faster rate. Against this backdrop, steel modular building systems (MBSs), underpinned by modern methods of construction (MMC), design for manufacturing and assembly (DfMA) methodology, and design for disassembly/deconstruction (DfD)

considerations, are becoming an increasingly compelling solution to the construction industry owing to the excellent strength-to-weight ratio of structural steel [2] and well-established advantages of modular construction, such as halved construction times [3], lower upfront costs [4], reduced waste generation [5], demountability and reusability [6], reduced on-site labour [7], safer work sites [8], and better quality control [9]. As shown in Fig. 1, in volumetric modular construction, prefabricated building units are prefabricated offsite in a controlled factory environment and then delivered to site for final assembly through bolted (or other types of) inter-module connections (IMCs) to form a fully finished building.

* Corresponding author.

E-mail address: konstantinos.tsavdaridis@city.ac.uk (K.D. Tsavdaridis).

<https://doi.org/10.1016/j.engstruct.2023.116121>

Received 1 January 2023; Received in revised form 7 March 2023; Accepted 5 April 2023

Available online 16 April 2023

0141-0296/© 2023 The Authors. Published by Elsevier Ltd. This is an open access article under the CC BY license (<http://creativecommons.org/licenses/by/4.0/>).

For economies of scale, steel MBSs are ideal for tall building applications with repeated units, such as apartments, student residences, and hotels [9]. Nevertheless, their application to date mostly concerns multistorey buildings [10], with the optimal number of floors being usually around six. Arguably, this predominance is attributed to the fact that the structural behaviour of tall MBSs in terms of serviceability and integrity under extreme environmental loads from high winds (as well as earthquakes) is generally more complex and less well understood than conventional building structures. In particular, the column discontinuity introduced by the IMCs between stacked modules (see Fig. 1(b)) reduces the overall lateral stiffness of MBSs and increases the effective (buckling) length of the corner posts. The former renders the structures more susceptible to large static and dynamic structural responses under wind effects, causing serviceability issues (e.g., damage to non-structural components and wind-induced occupant discomfort), whereas the latter makes the structures more vulnerable to member and/or global instability under combined gravitational and extreme wind loads. Still, there are exceptional examples of MBSs reaching over 130 m, such as the recently completed 150 m tall College Road project in Croydon, the UK (Fig. 1. (d)). In these cases, however, the buildings achieve structural integrity and stability through hybrid structural systems that consist of stacked modules arranged around a reinforced concrete core [11,12], with the modules designed to carry gravitational loads only. Nevertheless, the concept of tall self-standing (i.e., a fully-modular superstructure without any additional lateral stability system) MBSs is deemed worthy of investigation because of its shorter construction cycle, as in this case on-site erection of a separate/additional lateral load resisting system (LLRS) is not required. Despite the growing momentum of MBSs in the literature, the existing body of work concerning with this notion is still limited, with studies mostly focusing on the effect of static and cyclonic wind loading on the lateral drift performance of steel MBSs between 8 and 11 stories [13–16].

On the other hand, another challenge that may have hindered the development of taller self-standing modular buildings is the increase in structural material consumption required for stiffening and strengthening the individual modules to sustain larger gravitational and wind actions as the buildings get higher. Although this is generally true for all tall building structures [19], the increasing effect of building altitude on the structural material usage/costs and member sizes may be more severe for tall MBSs because of doubled beams and bundled columns from

adjacent modules (see Fig. 1 (c)). Moreover, due to column discontinuity at IMCs, the structural members of individual modules need to be adequately stiff and large to prevent column instability under combined gravitational and lateral loads, which can further increase the overall steel tonnage. In this regard, the impact of satisfying performance-based wind design criteria on the LLRS self-weight also remains unclear for tall self-standing MBSs. Note that this topic may also be critical for sustainability reasons, as the upfront cost and environmental impacts of tall buildings are closely related to their structural material usage. Currently, the manufacture of building materials accounts for about 11% of total greenhouse gas emissions [20]. For tall buildings in particular, a large proportion of their embodied carbon emissions (during material production, construction, maintenance, and demolition) is almost always produced by their LLRS [21]. As a result, the need to investigate the structural efficiency (broadly defined here as the ratio of certain structural utility to material consumption) of tall self-standing MBS is genuine in order to foster an economical and sustainable solution to the ongoing housing crisis. By designing for minimum weight in a performance-based context, the structural material consumption of steel MBS can be reduced, leading to an equivalent embodied carbon reduction [22] and a further decrease in upfront costs (note that currently MBSs are already 10% to 20% cheaper [4]). For conventional building structures, their minimum-weight designs are typically achieved through experiential trial-and-error design cycles [23] or performance-based design optimisation approaches [24–28]. When designing for wind loads, the sizing of their LLRS is generally governed by serviceability considerations rather than member resistance [29], which may explain why most sizing frameworks for conventional building structures (such as those listed above) primarily concern serviceability issues. However, this may not be the case for tall self-standing modular buildings due to their sensitivity to geometric nonlinear effects. Under combined gravitational and wind loads, their member forces can be significantly magnified by structural and member deformations as demonstrated later in this study. Consequently, this nonlinearity must be properly accounted for in the structural analysis/optimisation to accurately evaluate strength constraint functions. To this end, applying conventional sizing frameworks directly to self-standing modular structures may lead to various issues, such as difficulty in meeting both serviceability and member strength criteria simultaneously, slow convergence due to a large number of structural members and design

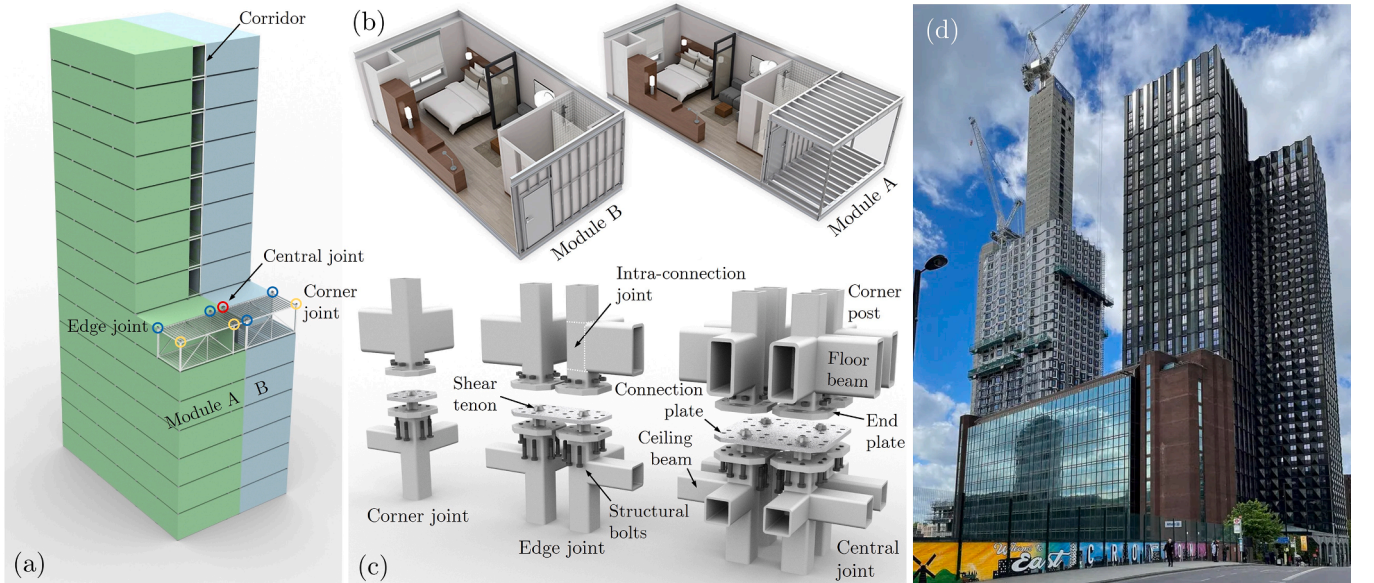


Fig. 1. (a) illustration of a typical tall self-standing MBS comprising corner, edge, and internal IMCs, (b) illustration of two completed modular units [17], (c) assembly view of corner, edge, and internal IMCs for the sizing design investigation in this study, and (d) College Road project during construction [18].

variables, and premature termination of the sizing process during geometrically nonlinear analysis (see detailed discussion of these issues in Section 3.2).

To this end, this study proposes a performance-based sizing design framework (Section 3.1) for LLRS weight reduction of tall self-standing MBSs subjected to multiple SLS and ULS design constraints under static and dynamic wind loads. The framework relies on a sizing optimisation problem formulation that considers codified drift- and floor-acceleration-based serviceability criteria, together with member strength requirements for structural integrity. A numerical solution strategy is devised (Section 3.2) to facilitate meaningful and computationally efficient solutions to the proposed weight minimisation problem by decomposing the sizing workflow into the SLS and ULS stages. The latter can then be solved sequentially and independently using any combination of well-established local and global optimisation algorithms. For demonstration, an adapted interior-point method (IPM) for continuous sizing design under static and dynamic serviceability constraints is provided in Section 4.1, while a genetic algorithm (GA) for discrete sizing design under member strength constraints is presented in Section 4.2. A numerical application of the sizing framework, entailing the IPM and GA in Section 4, to a representative 15-storey self-standing steel modular building under three levels of wind intensity is provided in Section 5 to demonstrate the applicability and potential gains. The continuous and discrete sizing are achieved by a custom engineering application developed using the Open Application Programming Interface (OAPI) of SAP2000, enabling the integration of SAP2000 for structural analysis and MATLAB for constrained structural optimisations. The optimal (sizing) designs of the adopted building are comprehensively assessed in Section 6 in accordance with Eurocode 3 [30], shedding light on the elastic stability behaviour, effects of geometric nonlinearity on wind-induced responses, and impacts of global geometric imperfections on member utilisation ratios of the case-study building under combined gravitational and wind loads. Finally, Section 7 summarises the main conclusions. In the next section, the limit state design considerations for steel tall MBSs under wind effects are discussed.

2. Limit state design considerations for tall Self-Standing MBSs under wind effects

Currently, there is a lack of specific design standards for MBSs, so the current design practice is generally based on the regulations for conventional building structural systems. However, since modular buildings are still building structures, the common limit state design considerations for conventional buildings should still be applicable to MBSs, which must satisfy the same, if not more stringent, standards of serviceability and safety [31].

To this end, tall buildings, loosely defined as those exceeding 50 m or 14 stories [32], are generally susceptible to two types of serviceability issues caused by excessive wind-induced deformations and oscillations [33,34] owing to their increased lateral flexibility and low inherent damping [29]. The first one is related to non-structural damage (to partition walls, windows and door frames, ceilings, and external cladding/facades) due to large inter-storey drifts and/or overall deflection in the along-wind (drag) direction, which are induced by the mean/static wind pressures and thus often referred to as static serviceability criteria. For instance, the limits of $H/600$ for the total building drift and $h/500$ for the inter-storey drift were specified by Griffis [35], where H is the total building height and h is the storey height. The second problem concerns building occupant discomfort caused by excessive floor acceleration in the across-wind (lift) direction, which is induced by structural resonance with the vortex shedding phenomenon [36,37], and is often referred to as the dynamic serviceability criterion. In this regard, many design protocols (e.g., ISO6897:1984 [38], ALJ-GEH-2004 [39]) have prescriptive provisions for regulating occupant comfort/habitability performance of tall buildings under wind excitation. This is

usually achieved by requiring the maximum wind-induced floor acceleration, either peak or root mean square (RMS), associated with a given recurrence interval to be below a codified threshold value depending on the building's fundamental frequency of the dominant translational mode [29,40]. According to a rough criterion by the ASCE 7–95 Standard [41], a building can be considered laterally flexible and thus prone to the above serviceability issues when the ratio of building height to the least horizontal dimension exceeds 4, or when the fundamental natural frequency is less than 1 Hz. However, for tall rectangular buildings with aspect ratios (i.e., height over breath) >3 , the dynamic serviceability issue in the across-wind direction is generally more critical than the static drift issue in the along-wind direction, thereby governing the wind-related serviceability design [42,43].

Finally, while the above serviceability issues concern wind-induced responses at the global level, tall building designs under strong winds may also be governed at the local/member level by strength requirements on member resistance. Specifically, verification of buckling resistance is crucial for slender structural members to ensure member stability under combined gravitational and wind loads. In this regard, geometric nonlinear effects may need to be considered in the analysis to accurately determine the member design forces, with appropriate allowances also to account for the effects of global and local/member imperfections (see Eurocode 3 [30]).

3. Performance-based optimal design problem formulation and efficient numerical solution strategy

3.1. Sizing optimisation problem formulation for minimum structural weight

The general form of the weight minimisation problem of building structures comprising n (or n groups of) frame members subjected to m performance constraints can be stated as follows

$$\begin{aligned} \min_{\mathbf{a}} \left\{ M(\mathbf{a}) = \sum_{i=1}^n \rho_i l_i a_i \right\} \\ \text{subject to } c_j(\mathbf{a}) \geq 0 \text{ for } j = 1, \dots, m, \\ \mathbf{a}^{\min} \leq \mathbf{a} \leq \mathbf{a}^{\max}, \end{aligned} \quad (1)$$

where $\mathbf{a} \in \mathbb{R}^n$ is the design variables (DVs) taken as the cross-sectional areas of frame members and bounded by side constraint $\mathbf{a}^{\min} \leq \mathbf{a} \leq \mathbf{a}^{\max}$, $M(\mathbf{a}) : \mathbb{R}^n \rightarrow \mathbb{R}$ is the objective function taken as the self-weight of the building's LLRS, $c_j(\mathbf{a}) : \mathbb{R}^n \rightarrow \mathbb{R}$ is the j -th performance constraint, and ρ_i and l_i denote the material density and length of frame member i , respectively. In the above formulation, the DVs \mathbf{a} can be continuous, discrete, or mixed. Importantly, only cross-sectional areas are selected as the DVs here. This consideration facilitates the weight-minimal design formulation in Eq. (1) and is supported by expressing all other sectional properties (contributing to the overall building stiffness) in terms of the cross-sectional area only (see Section 5).

To support the performance-based sizing design of tall self-standing MBSs under wind effects, this study considers wind-induced drift and floor acceleration constraints for SLS, and member strength constraints for ULS. Specifically, for a k -storey building (with floor k being the roof), the along-wind inter-storey drift and roof displacement constraints in Eq. (1) take the forms of

$$\begin{aligned} c_j(\mathbf{a}) = -|\Delta_j(\mathbf{a})| + \Delta_{\text{lim}} \geq 0, \quad \forall j = 1, \dots, k, \\ \text{and} \\ c_{k+1}(\mathbf{a}) = -|u_k^{\text{clg}}(\mathbf{a})| + u_{\text{lim}} \geq 0, \end{aligned} \quad (2)$$

respectively, where $\Delta_j(\mathbf{a})$ and $u_k^{\text{clg}}(\mathbf{a})$ are the inter-storey drift ratio for storey j and the lateral displacement at the building roof, respectively, and Δ_{lim} and u_{lim} are the corresponding codified permissible limits. Here, the inter-storey drift ratios are defined as $\Delta_j = (u_j^{\text{clg}} - u_j^{\text{flr}})/h_j$, where u_j^{clg} and u_j^{flr} are the wind-induced lateral

displacements at the ceiling and floor levels of storey j , respectively, and h_j is the corresponding storey height.

For across-wind floor accelerations, the constraint functions are specified by

$$c_j(\mathbf{a}) = -\left| \ddot{u}_j^{\text{flr}}(\mathbf{a}) \right| + \ddot{u}_{\text{lim}}(f_1) \geq 0, \quad \forall j = k+2, \dots, 2k, \quad (3)$$

in which $\ddot{u}_j^{\text{flr}}(\mathbf{a})$ is the wind-induced lateral acceleration at the floor level of storey j , and $\ddot{u}_{\text{lim}}(f_1)$ is the codified acceleration threshold commonly defined as a function of the building's natural frequency of the first (or dominant) lateral vibration mode, f_1 [24]. Note that the unoccupied roof (or floor k) is excluded from the last equation, as its acceleration level does not affect occupant comfort under wind excitation.

Finally, for verification of member resistances under along-wind static loads, the strength constraints are given by

$$c_j(\mathbf{a}) = -r_j(\mathbf{a}) + 1 \geq 0, \quad \forall j = 2k+1, \dots, 2k+n, \quad (4)$$

where r_j is the maximum utilisation ratio for member (or member group)

j from all wind-related ULS load combinations. In this setting, there are $2k$ SLS constraints in Eq. (1) in total, comprising $k+1$ drift and $k-1$ acceleration constraints, plus n strength constraints, coming from n structural DVs.

3.2. Efficient numerical solution strategy

From the outset, the optimisation problem in Eq. (1) is nontrivial and computationally challenging to solve for three reasons.

- (1) All three types of performance constraints in Section 3.1 are generally non-convex [44], making the numerically more efficient local optimisation methods unsuitable for the task because they can be trapped in local optima.
- (2) For large structural systems with many DVs (such as tall MBSs), population-based global optimisation methods (e.g., GA) can be prohibitively slow because their optimisation performance is crucially dependent on population size [45], which in turn depends on the number of DVs. Although these heuristic methods

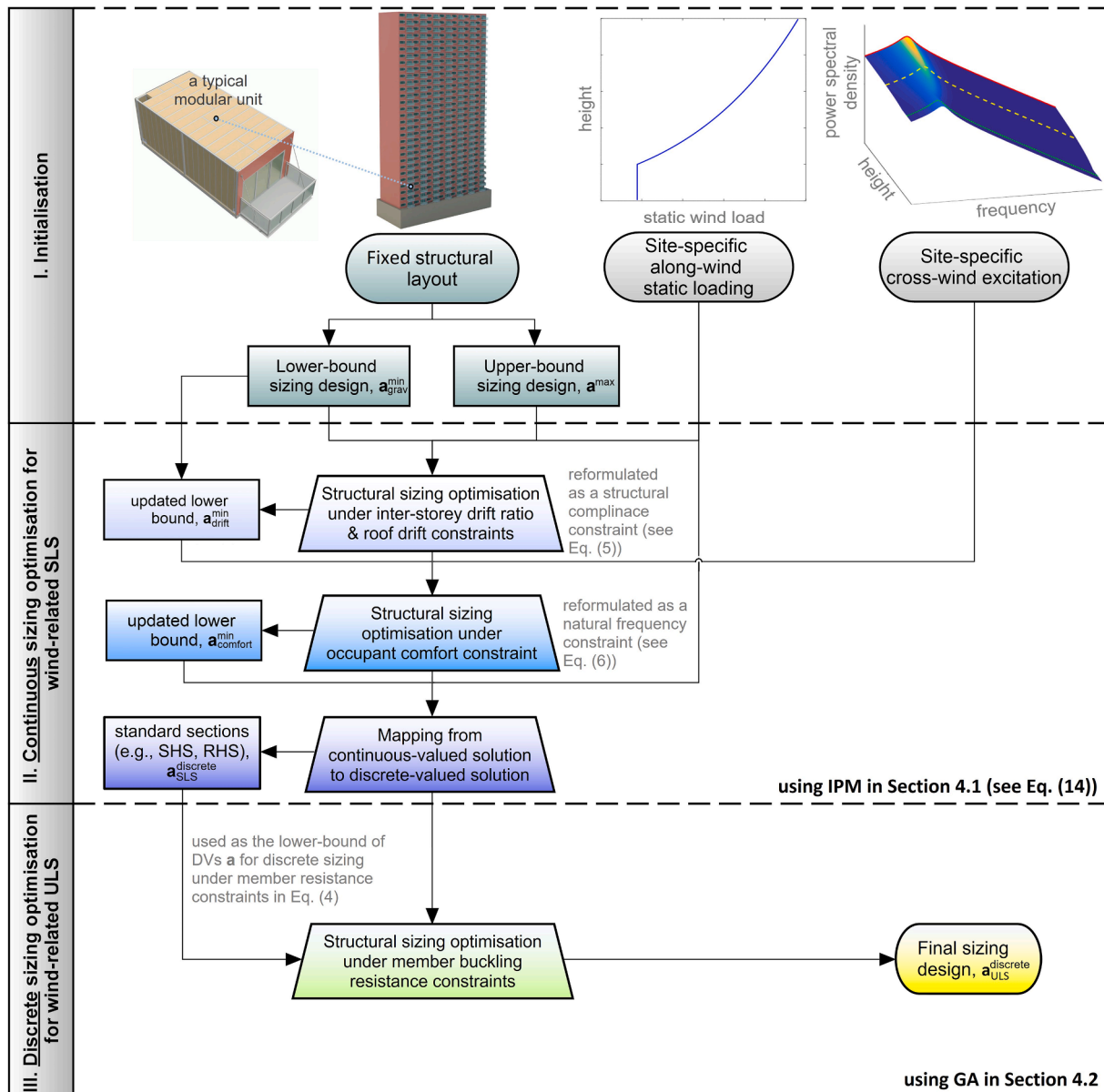


Fig. 2. Flowchart of solution strategy for minimal-weight design of tall MBSs subject to wind-related serviceability and ultimate limit state design constraints.

do not require gradient information, expensive evaluations of nonlinear performance constraints for a large number of candidate sizing designs are required to arrive at the final sizing design.

- (3) Compared to conventional building structures, tall self-standing MBSs are more prone to global and member instabilities when subjected to combined gravitational and lateral loads [46]. This is because the buckling lengths of the corner posts are increased by the discontinuity introduced by the IMCs (see Fig. 1(b)). Consequently, the effect of geometric nonlinearity (associated with structural and member deformations) on magnifying wind-induced member forces is more profound, and large-displacement analysis based on load incrementation strategies may be required to accurately evaluate member design forces for strength verification. However, this may lead to slow convergence or even failure when a candidate sizing design being analysed becomes structurally unstable before a specified ULS combination of loads is reached, causing the sizing optimisation process to terminate prematurely.

In view of the above challenges, a computationally efficient numerical strategy, as shown in Fig. 2, is developed herein to solve the weight-minimisation problem in Eq. (1). Specifically, the strategy addresses the above three challenges through implementing the following three techniques, separately:

- (i) The two non-convex SLS constraints in Eqs. (2) and (3) are first converted to a convex structural compliance constraint on the wind-induced strain energy and a convex natural frequency constraint on the building's first translational vibration mode as

$$c_{\text{compl}}(\mathbf{a}) = \sum_{j=1}^k (F_{w_j}^{\text{clg}} u_j^{\text{clg}} + F_{w_j}^{\text{flr}} u_j^{\text{flr}}) - E_{\text{lim}} \leq 0, \quad (5)$$

and

$$c_{\text{freq}}(\mathbf{a}) = f_1(\mathbf{a}) - f_{\text{target}} \geq 0, \quad (6)$$

respectively. In Eq. (5), $F_{w_j}^{\text{clg}}$ and $F_{w_j}^{\text{flr}}$ denote the static along-wind loads lumped at the ceiling and floor levels of storey j , respectively, while E_{lim} is the upper-bound elastic strain energy selected as the measure of static lateral stiffness of the building. A good estimate of E_{lim} can be found by $E_{\text{lim}} \approx F_{w_j}^{\text{clg}} u_{j,\text{lim}}^{\text{clg}} + F_{w_j}^{\text{flr}} u_{j,\text{lim}}^{\text{flr}}$, where $u_{j,\text{lim}}^{\text{clg}}$ and $u_{j,\text{lim}}^{\text{flr}}$ are the lateral displacement limits at the ceiling and floor levels of storey j , respectively, converted from the code-specific inter-storey drift requirements. Moreover, f_{target} in Eq. (6) is the lower-bound (target) frequency selected as the measure of dynamic lateral stiffness of the building, which can be found either analytically [24] or by trial and error [19]. By implementing technique (i), the two serviceability constraints become strictly convex [47], thus addressing challenge (1) at least partially (due to the strength constraints in Eq. (4) still being nonconvex).

(ii) After converting the two SLS constraints, the optimisation problem in Eq. (1) is decoupled into two sequential stages: a convex SLS stage and a non-convex ULS stage. This decomposition allows for convenient and sequential solutions to the two staged subproblems using preferred local and global sizing algorithms, separately. In this arrangement, the MBS is first optimised for lateral stiffness to meet the converted drift and floor acceleration constraints, and then for member resistance to satisfy the strength requirements. Upon optimally stiffening a modular building for serviceability criteria, a large number of its structural members (or member groups) are no longer governed by strength requirements. Consequently, the number of active DVs in the ULS stage of the sizing workflow significantly decreases, which, in turn, reduces the population size used by GA and hence improves computational efficiency, thus addressing challenge (2).

(iii) In the ULS stage of the proposed sizing workflow, the optimal design from the SLS stage, which satisfies the two serviceability

constraints, is used as the lower bound of the side constraint on the DVs \mathbf{a} . This manipulation reduces the likelihood of member instability issues during the geometrically nonlinear structural analysis in the ULS stage, thus addressing challenge (3).

At this point, the proposed solution strategy for the optimisation problem in Eq. (1) is outlined as follows. The workflow begins with initialisation, during which the building is first designed to meet all SLS and ULS criteria for gravitational loads only using standard structural design methods. For wind-sensitive modular buildings, this design will most likely not meet the codified serviceability and strength criteria, thereby necessitating further stiffening and strengthening through resizing. The member sizes of this design, indicated as $\mathbf{a}_{\text{grav}}^{\text{min}}$ in Fig. 2, are used as the initial lower bound of the side constraint for the sizing optimisation under drift constraints. The upper bound of the DVs, denoted as \mathbf{a}^{max} in Fig. 2, can be established based on architectural, functional, and other buildability considerations.

After initialisation, the workflow proceeds to the sizing optimisation under the drift constraints in Eq. (2), which are now converted to a single compliance constraint defined in Eq. (5). This optimisation aims to find the optimal set of DVs, $\mathbf{a}_{\text{drift}}^{\text{min}}$, within the initial side constraint, $\mathbf{a}_{\text{grav}}^{\text{min}} \leq \mathbf{a} \leq \mathbf{a}^{\text{max}}$, by experientially adjusting E_{lim} value in Eq. (5) until the two sets of drift criteria in Eq. (2) are simultaneously met. Once $\mathbf{a}_{\text{drift}}^{\text{min}}$ is found, it is used as the new starting point and lower bound, i.e., $\mathbf{a}_{\text{drift}}^{\text{min}} \leq \mathbf{a} \leq \mathbf{a}^{\text{max}}$, for the subsequent sizing optimisation under floor acceleration constraints in Eq. (3), which are now converted to a natural frequency constraint in Eq. (6). This optimisation aims to find the optimal set of DVs, $\mathbf{a}_{\text{drift}}^{\text{min}}$, within the updated side constraint, $\mathbf{a}_{\text{drift}}^{\text{min}} \leq \mathbf{a} \leq \mathbf{a}^{\text{max}}$, to satisfy the acceleration constraints. Importantly, the two sequential sizing processes in the SLS stage are both continuous-valued; the discrete optimal sections, $\mathbf{a}_{\text{SLS}}^{\text{discrete}}$, are only specified/selected (per member design groups) after $\mathbf{a}_{\text{comfort}}^{\text{min}}$ is determined. This is achieved by mapping the obtained continuous cross-sectional properties onto different catalogues of commercially available steel sections (see Section 5 for demonstration).

Finally, the sizing workflow progresses to the ULS stage, in which $\mathbf{a}_{\text{SLS}}^{\text{discrete}}$ is used as the new starting point and lower bound in the discrete sizing process under member strength constraints for ULS load combinations associated with static along-wind forces. The optimisation process aims to determine the optimal set of standard sections, $\mathbf{a}_{\text{ULS}}^{\text{discrete}}$, that minimises $M(\mathbf{a})$ while satisfying the member strength constraints in Eq. (4). The determined sections are adopted as the final optimal solution to the weight-minimisation problem in Eq. (1) subjected to concurrent performance constraints in Eqs. (2), (3), and (4).

The applicability of the above solution strategy is illustrated in Section 5 using a 15-storey self-standing modular building exposed to different wind intensities, for which a numerical implementation of the sizing workflow is required. To this end, the following section details one local and one global optimisation algorithms for the SLS and ULS stages of the sizing workflow, separately. First, an IPM is presented in Section 4.1 for continuous sizing optimisation under convex serviceability constraints. Then, a GA is outlined in Section 4.2 for discrete sizing optimisation under nonconvex strength constraints. It is worth noting that the two algorithms presented next are just two possible choices and can be replaced by other local and global optimisation methods deemed appropriate.

4. Local and global optimisation algorithms for minimum-weight design of frame structures under convex and nonconvex performance constraints

4.1. Interior point method-based continuous sizing under convex structural compliance and natural frequency constraints

When subject to the convex compliance and frequency constraints,

the sizing optimisation problem in Eq. (1) is strictly convex. To solve this problem, one can convert the original optimisation problem in Eq. (1), with reformulated serviceability constraints in Eqs. (5) and (6), into an equivalent, unconstrained form by replacing the constraint functions with barrier terms. This results in an unconstrained optimisation problem that can be solved using deterministic local optimisation algorithms, such as the IPM [47] detailed in this section. Specifically, the unconstrained approximate problem for Eq. (1) subject to the compliance and/or frequency constraint can be formulated as

$$\min_{\mathbf{a}} \{B(\mathbf{a}, \mu)\} = \min_{\mathbf{a}} \left\{ M(\mathbf{a}) - \mu \sum_{l=1}^m \ln(c_l(\mathbf{a})) \right\}, \quad (7)$$

where $B(\mathbf{a}, \mu)$ is the barrier function, μ is a small positive scalar, and $\ln(c_l(\mathbf{a}))$ is the l -th barrier term, which is not defined for $c_l(\mathbf{a}) \leq 0$ and is restricted to be positive during the sizing iteration. In case only one constraint (either compliance or frequency) is considered at a time (which is the case in the current study), the number m in the last equation reduces to 1 and the summation on l drops. Evidently, as μ decreases to zero, the barrier function $B(\mathbf{a}, \mu)$ degenerates to the original objective function $M(\mathbf{a})$ such that the minimum of $B(\mathbf{a}, \mu)$ should approach the solution of Eq. (1). Accordingly, instead of solving Eq. (1) directly, it is equivalent to solve the approximate problem in Eq. (7) for given μ . Mathematically, this is equivalent to finding the stationary point of $B(\mathbf{a}, \mu)$ at which the gradient of $B(\mathbf{a}, \mu)$ equals to zero, i.e.,

$$\nabla_{\mathbf{a}} B(\mathbf{a}, \mu) = \nabla_{\mathbf{a}} M(\mathbf{a}) - \mu \sum_{l=1}^m \frac{\nabla_{\mathbf{a}} c_l(\mathbf{a})}{c_l(\mathbf{a})} = \mathbf{0}, \quad (8)$$

To solve Eq. (8), Lagrange multiplier-like dual variables, stored in vector $\boldsymbol{\lambda} = \{\lambda_1, \dots, \lambda_m\}^T$ (where “ T ” denotes transpose operation), are next introduced in the following equality

$$\mu = \lambda_l c_l(\mathbf{a}) \quad (l = 1, \dots, m), \quad (9)$$

through which Eq. (8) can be rewritten in the vector–matrix form as

$$\nabla_{\mathbf{a}} M(\mathbf{a}) - \mathbf{J}^T \boldsymbol{\lambda} = \mathbf{0}, \quad (10)$$

where $\mathbf{J} \in \mathbb{R}^{m \times n}$ is the Jacobian matrix of the constraint function $\mathbf{c} = \{c_1(\mathbf{a}), \dots, c_m(\mathbf{a})\}^T$. To solve for $(\mathbf{a}, \boldsymbol{\lambda})$, the Newton-Raphson method is applied to Eqs. (9) and (10) to give

$$\begin{bmatrix} \mathbf{H}_B & -\mathbf{J}^T \\ \boldsymbol{\Lambda} \mathbf{J} & \mathbf{C} \end{bmatrix} \begin{Bmatrix} \mathbf{d}_a \\ \mathbf{d}_\lambda \end{Bmatrix} = \begin{Bmatrix} -\nabla M(\mathbf{a}) + \mathbf{J}^T \boldsymbol{\lambda} \\ \boldsymbol{\mu} \mathbf{1} - \mathbf{C} \boldsymbol{\lambda} \end{Bmatrix}, \quad (11)$$

in which $\mathbf{H}_B \in \mathbb{R}^{n \times n}$ is the Hessian matrix of $B(\mathbf{a}, \mu)$, $\boldsymbol{\Lambda} \in \mathbb{R}^{m \times m}$ and $\mathbf{C} \in \mathbb{R}^{m \times m}$ are the diagonal matrices of λ and \mathbf{c} , respectively, $\mathbf{1} \in \mathbb{R}^{m \times 1}$ is a unit vector, and $\mathbf{d}_a \in \mathbb{R}^{n \times 1}$ and $\mathbf{d}_\lambda \in \mathbb{R}^{m \times 1}$ are the search directions for the primal and dual variables, \mathbf{a} and $\boldsymbol{\lambda}$, respectively. Because μ and $c_l(\mathbf{a})$ are both positive, the condition $\boldsymbol{\lambda} \geq \mathbf{0}$ must be enforced at each iteration (because of Eq. (9)). Finally, for a given value of μ , the sizing DVs and the Lagrangian multipliers, \mathbf{a} and $\boldsymbol{\lambda}$, can be found through iteration using the following formula

$$\begin{Bmatrix} \mathbf{a} \\ \boldsymbol{\lambda} \end{Bmatrix}^{(p+1)} = \begin{Bmatrix} \mathbf{a} + \alpha \mathbf{d}_a \\ \boldsymbol{\lambda} + \alpha \mathbf{d}_\lambda \end{Bmatrix}^{(p)}, \quad (12)$$

where α is the step size at the iteration step p , which can be determined by, e.g., the merit function method [48]. The above iteration is then executed until the following convergence criteria are satisfied within a prespecified tolerance, ε_{tol} ,

$$\begin{aligned} \left| \frac{\partial M(\mathbf{a})}{\partial a_i} - \sum_{l=1}^m \lambda_l \frac{\partial c_l(\mathbf{a})}{\partial a_i} \right| &\leq \varepsilon_{\text{tol}} \quad (i = 1, \dots, n) \text{ and} \\ |c_l(\mathbf{a})| &\leq \varepsilon_{\text{tol}} \quad (l = 1, \dots, m) \end{aligned} \quad (13)$$

4.2. Genetic algorithm-based discrete sizing under nonconvex member strength constraints

Structural sizing problems under elemental stress constraints are generally non-convex, with several local optima having different objective function values [44]. For volumetric modular buildings, their modular units generally use standard hollow sections such that the sizing DVs in Eq. (1) can only attain discrete values. To this end, a global, discrete sizing algorithm, such as GA [49], is needed for the minimum-weight design of tall MBSs under code-prescribed member strength constraints in Eq. (4). Specifically, GAs apply the principle of survival of the fittest to a population of potential solutions/individuals to produce a successively improved population of solutions to a given optimisation problem. At each generation, a new set of solutions (known as offspring) is generated by selecting better-fit individuals in the current population (known as parents) based on their fitness levels and then allowing them to reproduce via genetics-inspired operations, such as crossover and mutation. GAs are also applicable to integer optimisation problems, making them suitable for the automatic selection of cross-sections to meet member strength requirements. In this context, an integer GA adapted from Deep et al. [50] is presented herein for the discrete sizing design of tall MBSs subject to strength constraints on the buckling resistance of members according to Eurocode 3 [30]. For this task, the DVs in Eq. (1) can only be selected from sets of discrete values based on the cross-sectional areas of the standard sections made available for the discrete sizing optimisation. This is achieved conveniently by introducing the integer DVs $\mathbf{x} \in \mathbb{Z}_+^n$ (where \mathbb{Z}_+ denotes the set of positive integers), which are linked to the sizing DVs, \mathbf{a} , through a one-to-one correspondence. The former DVs contains n location indices of the cross-sections (for n groups of modular members) in their corresponding lists of standard candidate sections. For volumetric modular buildings, hot-finished rectangular hollow sections (RHS) are generally used for modular beams, while hot-finished square hollow sections (SHS) are used for corner posts/bracings. The adapted GA is described in the following steps.

- (1) Generate a sufficiently large initial set of random designs with population size m (based on the number of DVs) within the design domain confined by the side constraint, $\mathbf{x}^{\min} \leq \mathbf{x} \leq \mathbf{x}^{\max}$, where \mathbf{x}^{\min} and \mathbf{x}^{\max} are the lower and upper bounds of the location indices.
- (2) Check if the maximum number of generations is reached or if the relative change in the best fitness function value over a pre-specified number of generations is less than a pre-specified tolerance. If any of the two conditions is met, stop the GA; else proceed to step (3). The fitness function of individual/candidate design i in a generation, $f(\mathbf{x}_i) \in \mathbb{R}^n \rightarrow \mathbb{R}$, is defined based on the feasibility approach by Deb [49] as

$$f(\mathbf{x}_i) = \begin{cases} M(\mathbf{x}_i), & \text{if } \mathbf{x}_i \text{ is feasible;} \\ M_{\text{worst}} + \sum_{j=1}^m c_j(\mathbf{x}_i), & \text{otherwise,} \end{cases} \quad (14)$$

where M_{worst} is the objective function value of the worst feasible solution in the current population, and the summation term, $\sum c_j(\mathbf{x}_i)$, reflects the total degree of performance constraint violations. If there is no feasible solution in the current population, M_{worst} is set to zero.

- (3) Apply the k -way deterministic tournament selection [51] (with a tournament size k , note $k < m$) to the current population to create a mating pool. To this aim, k individuals are selected randomly from the current population for a tournament, with the “champion” of the tournament (the one with the lowest $f(\mathbf{x}_i)$ value) placed in the mating pool. This procedure is executed systematically and repeatedly until each individual in the current

population participates in k tournaments exactly. Evidently, the fittest individual/design in the current generation wins all k tournaments and makes k copies of itself in the mating pool, whereas the least-fit individual loses all k tournaments and is thus eliminated. In this way, the mating pool always remains the same size as the current population (i.e., m), with better-fit individuals having a higher chance of being included multiple times.

- (4) To create a new set of populations, a probabilistic crossover operation is next applied, with probability $P_c \in [0,1]$, to $m/2$ pairs of parents in the mating pool from step (3) to generate m offspring, forming the next generation. For $P_c \neq 0$, the above operation recombines the parents' genes to reproduce two new solutions from each parenting pair, whereas for $P_c = 0$, no crossover is applied and two parents are directly cloned into the offspring generation. Herein, the extended Laplace crossover operator proposed by Deep et al. [50] is adopted to generate two offspring, \mathbf{x}^{o1} and \mathbf{x}^{o2} , from two randomly selected parents, \mathbf{x}^{p1} and \mathbf{x}^{p2} , as follows. First, a random parameter, β_i , satisfying the Laplace distribution, is generated for the i -th "chromosomes" (i.e., the i -th element of \mathbf{x}) of two offspring (where $i = 1, \dots, n$) as

$$\beta_i = \begin{cases} a - b \log(u_i), & r_i \leq 1/2; \\ a + b \log(u_i), & r_i > 1/2, \end{cases} \quad (15)$$

where a and $b > 0$ are two pre-defined parameters, and u_i and r_i are two random variables with a uniform distribution between 0 and 1. Then, the i -th chromosomes of two offspring, x_i^{o1} and x_i^{o2} , are generated using the equation below

$$\begin{aligned} x_i^{o1} &= x_i^{p1} + \beta_i |x_i^{p1} - x_i^{p2}|, \\ x_i^{o2} &= x_i^{p2} + \beta_i |x_i^{p1} - x_i^{p2}|. \end{aligned} \quad (16)$$

After the offspring are generated, a mutation operation, with probability $P_m \in [0,1]$, is next applied to all offspring following

$$x_i^{\text{mute},j} = \begin{cases} x_i^{oj} - (s_i^j)^q (x_i^{oj} - x_i^{\min}), & t < r, \\ x_i^{oj} + (s_i^j)^q (x_i^{\max} - x_i^{oj}), & t \geq r, \end{cases} \quad (17)$$

where $x_i^{\text{mute},j}$ denotes the muted chromosome i of offspring j ($j = 1, \dots, m$), x_i^{\min} and x_i^{\max} are the i -th entries of \mathbf{x}^{\min} and \mathbf{x}^{\max} , respectively, s_i^j is a random variable between 0 and 1, and $q > 1$ is the mutation parameter controlling the strength of the mutation.

- (5) Apply integer restrictions to the offspring with non-integer chromosomes, and then evaluate the fitness values of all offspring (with rounded chromosomes) according to Eq. (14). Specifically, the non-integer chromosomes, x_i^{mute} ($i = 1, \dots, n$), are rounded to either $\lfloor x_i^{\text{mute}} \rfloor$ or $\lfloor x_i^{\text{mute}} \rfloor + 1$, where $\lfloor x_i^{\text{mute}} \rfloor$ denotes the integer part of x_i^{mute} . This ensures greater randomness in the set of offspring being generated and avoids the same integer values being generated repeatedly for different offspring.
- (6) Increase the current generation number by 1, then go back to step (2).

In the numerical part of this work, the continuous and discrete sizing optimisations of the case-study building are achieved by a custom optimisation application developed using the OAPI of SAP2000, which allows for the integration of SAP2000 for structural analysis and MATLAB for structural optimisation. The IPM- and GA-based sizing optimisations presented in this section are implemented using MATLAB's built-in functions/solvers "fmincon" and "ga", respectively.

5. Minimum-weight design of a typical tall steel MBS under wind loads

5.1. Description of case-study building and design wind actions

To illustrate the applicability of the proposed sizing framework in Section 3, a 15-storey steel modular building shown in Fig. 3(a) is adopted as a representative structure of wind-sensitive self-standing modular buildings. The building is 53.5 m tall with a 26.1 m-by-17.2 m rectangular floor plan and comprises 180 modules in total (or 12 modules per storey) interconnected by corner, edge, and central IMCs. All modules share a constant width of 4.20 m and a height of 3.38 m but have two different lengths of 9.45 m and 7.60 m. For each module, floor and ceiling beams are welded directly to corner posts to form rigid intra-module connections, which is a common practice for prefabricated volumetric modules [52]. To increase the building's lateral and torsional stiffness, bracings are arranged in a limited number of modules at selected locations as shown in Fig. 3 (b) without affecting the usage of the internal space. In terms of cross-sections, corner posts and bracings are made of hot-finished SHS, while ceiling and floor beams are made of hot-finished RHS. A linear finite element model of the building is developed using SAP2000® v18 software, comprising 6,854 (1D) frame elements, 1,110 dummy area elements (for modelling façade and internal wall panels), and 900 rigid membrane elements (for modelling floor, ceiling, and roof panels). As shown in Fig. 3 (c), the corner, edge, and internal IMCs are modelled using short vertical frame elements with a hinge in the middle, which is released for biaxial bending. In addition, adjacent modules are horizontally interconnected at the edge and internal IMCs using one and six 2-joint link elements with six degrees of freedom, respectively, as shown in Fig. 3(c). All link elements are rigid in their local U_1 and U_2 directions, with their shear stiffness in local U_3 direction, bending stiffness about the local U_2 and U_3 axes, and torsional stiffness about the local U_1 axis all set to 0. For dynamic analysis, all six damping coefficients of the link elements are set to 0 for conservatism. Apart from the structural self-weight, additional gravitational design loads are estimated based on actual MBSs [53] and applied as uniformly distributed loads, as summarised in Table 1.

To support practicality and cost-efficiency, twenty member/design groups are considered for the building, with common cross-sections changing every three stories, yielding 20 sizing DVs in total as shown in Fig. 3 (a). The side dimensions of corner posts and bracings are restricted to be within the ranges of 180 to 350 mm and 100 to 260 mm, respectively, while the sectional depths of modular beams are restricted to be within the range of 120 to 400 mm. To prevent local buckling of modular members before attaining the yield strength, Class 4 sections are excluded from the ensuing sizing optimisations. This grouping of structural members is largely driven by fabrication considerations for volumetric modular buildings and partially by structural rationality. In general, it is preferable to standardise modular units by requiring the corner posts, floor and ceiling beams, and bracings in adjacent floors to use the same steel sections to ensure economies in manufacturing and material procurement processes [54].

Prior to sizing the building for wind loads, the building is first designed to satisfy all SLS and ULS requirements of Eurocode 3 [30] for gravitational load combinations in Table 1, prescribed by Eurocode 1 [55]. The cross-sections of this design (termed "initial design" from hereafter) with a self-weight of 280.3 metric tons are reported in Fig. 3 (b), which are used as the starting point and the initial lower bound for the side constraints on the sizing DVs in the subsequent displacement-based optimisation. The first three mode shapes of this design are obtained using standard linear modal analysis and plotted in Fig. 3(d), with the fundamental vibration mode being translational in the global y direction. The first three natural frequencies and the corresponding modal participating mass ratios in parentheses are 0.48 Hz (67.0%), 0.49 Hz (60.0%), and 0.53 Hz (73.0%), respectively. For later dynamic analysis, the structural damping for the fundamental mode is taken as 0.8%,

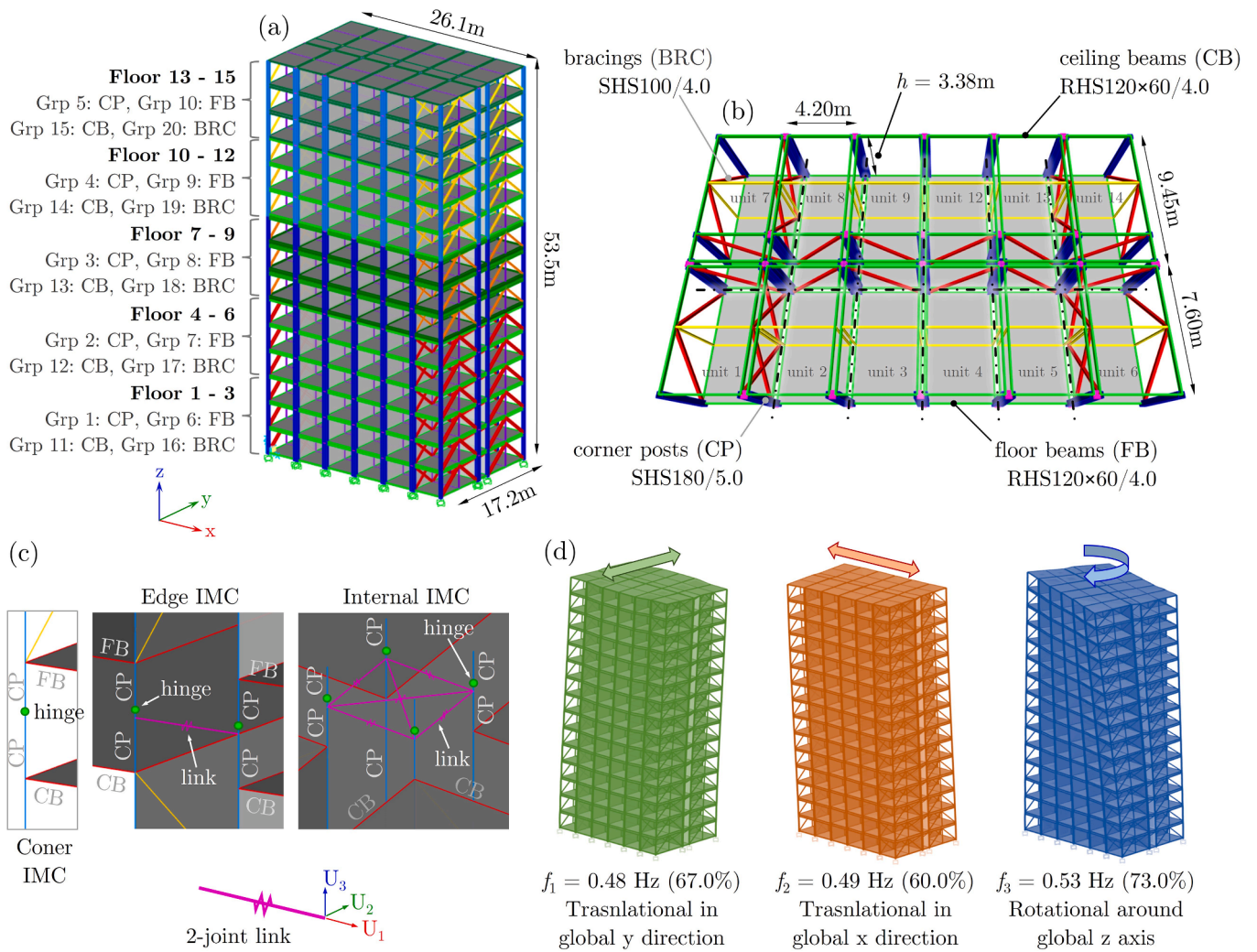


Fig. 3. (a) 15-storey case-study MBS and member design groups for the sizing optimisation investigation, (b) illustration of a typical floor, (c) simplified finite element models of corner, edge, and internal IMCs, and (d) the first three vibration modes of the case-study building.

Table 1

Selected load combinations based on Eurocode 1 and design loads for sizing optimisation of the case-study building under SLS and ULS design constraints according to Eurocode 3.

Design loads	Floor	Ceiling	Roof	Facade	Wall Panels
Superimposed load [kPa]	0.75	1.00	2.50	1.00	0.50
Live load [kPa]	2.00	/	1.00	/	/
Design load combinations	SLS		ULS		
Gravitational loads	1.0G + 1.0Q		1.35G + 1.5Q		
Gravitational & wind loads	1.0G + 1.0Q ± 0.6W _y		1.35G + 1.5Q ± 0.9W _y		
	1.0G + 0.7Q ± 1.0W _y		1.35G + 1.05Q ± 1.5W _y		

which closely follows the recommended value by Eurocode 1 [55] for steel buildings.

To assess the impact of wind intensity on the minimal sizing design of the case-study building, three basic reference wind velocities are considered in the numerical part of this work: $v_b = 25.0, 27.5,$ and 30.0 m/s. These reference velocities represent the 10-minute mean wind velocity at 10 m above open flat country terrain with a return period of 50 years. It is noteworthy that the adopted lower-bound velocity of 25.0 m/s is almost the minimum wind speed required for the case-study building in Fig. 3 (a) to be governed by wind effects. In contrast, the

upper-bound velocity of 30.0 m/s is already among the highest basic wind speeds on the mainland of Europe according to Eurocode 1 [55]. This allows for the investigation of various structural behaviours of the building under high wind conditions. Since the fundamental vibration mode of the adopted building is in the global y direction, along which the building's tributary width is also broader, the case-study structure is more critical in this direction for both wind-induced drift and floor acceleration. Consequently, the ensuing sizing optimisation only concerns this direction. Nevertheless, the same sizing process can also be performed in the global x direction if so desired. To this end, the static along-wind forces in the global y direction are calculated according to Eurocode 1 [55] assuming urban terrain, and plotted along the building height in Fig. 4 (a). The power spectral density (PSD) functions of the VS-induced cross-wind loads in the global y direction (with the wind coming in the global x direction) are estimated using the across-wind excitation model by Liang et al. [37] and plotted as continuous surfaces of the excitation frequency and elevation in Fig. 4(b).

Under the static along-wind loads in Fig. 4(a), the initial design reported in Fig. 3(b) is found to be deficient in meeting the total building drift limit of $H/600$ and the inter-storey drift limit of $h/500$ [35] for $v_b = 30$ m/s only, as shown in Fig. 4(c) and (d), respectively. Furthermore, under the dynamic across-wind loads in Fig. 4(b), the initial design with $f_1 = 0.48$ Hz is deficient in satisfying the occupant comfort stipulation by ISO6897:1984 [38] even for $v_b = 25$ m/s, as shown in Fig. 4(e). The above comfort threshold is specified by the wind-induced maximum

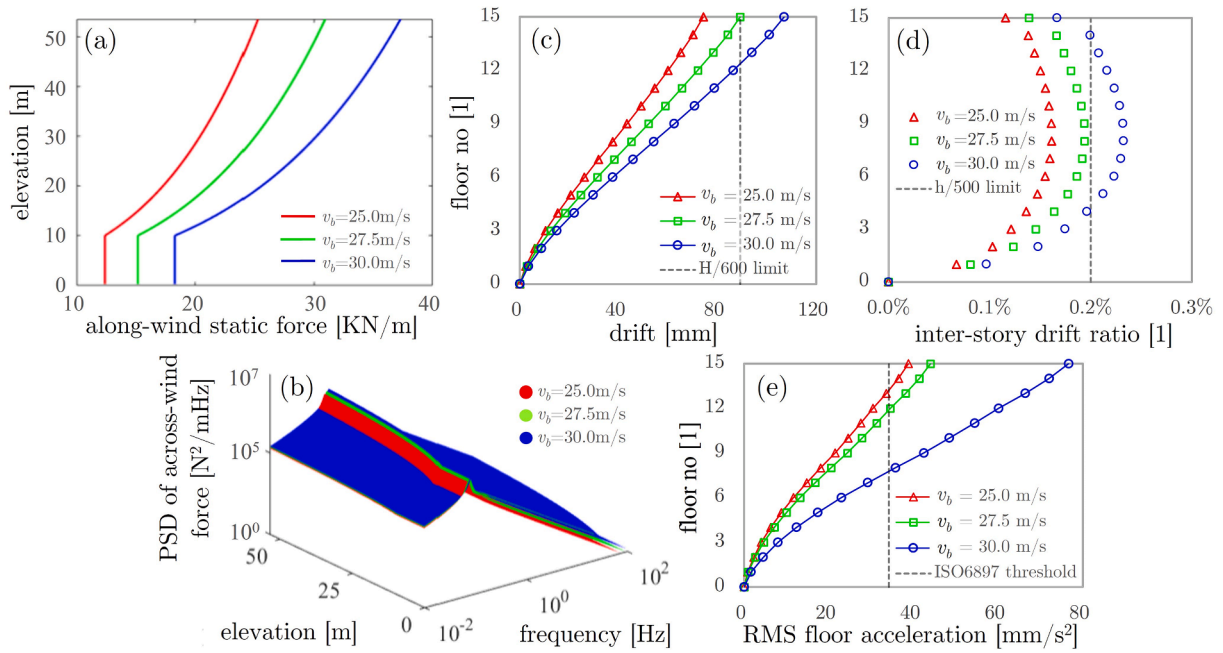


Fig. 4. (a) Static along-wind design forces, (b) power spectral density functions of across-wind design force, (c) long-wind drifts, (d) long-wind inter-storey drift ratios, and (e) across-wind floor accelerations of the case-study building in Fig. 3 (a) for basic wind speeds, 25.0, 27.5, and 30.0 m/s.

floor acceleration given in terms of the RMS value as

$$\ddot{u}_{lim}(f_i) = \exp(-3.65 - 0.41 \ln f_i), \quad (18)$$

which is plotted in Fig. 4(e). As seen, the threshold value remains unchanged for different wind speeds as it is only affected by the building's fundamental frequency. In view of Fig. 4 (c), (d), and (e), the case-study building in Fig. 3 (a) is indeed wind-sensitive, thereby requiring further stiffening (through resizing) to meet the above static and dynamic serviceability criteria.

5.2. Sizing optimisation under wind-induced drift and floor acceleration constraints

Specifically, for $v_b = 25.0$ and 27.5 m/s, the (continuous) sizing optimisation process under wind serviceability constraints starts directly with the floor acceleration constraints as the initial design in Fig. 3(b) is not governed by the wind drift limits. For $v_b = 30$ m/s, however, the sizing process starts with the drift limits first and then proceeds to the acceleration constraints. Still, all three sizing processes begin with the same initial design, with the cross-sectional areas (of the structural members) of this design being the lower bound of the initial side constraint, a_{grav}^{min} (see Fig. 2). The variation in the structural self-weight of the case-study building throughout the sizing process is plotted in Fig. 5 (a) for three basic wind speeds considered. As seen, the sizing iterations converge after 31, 53, and 79 steps for $v_b = 25.0, 27.5,$ and 30.0 m/s, respectively. The relative convergence tolerances for the objective function value (defined as $|M(\mathbf{a}^{(p+1)}) - M(\mathbf{a}^{(p)})| / M(\mathbf{a}^{(p+1)})$) and step size (defined as $|\mathbf{a}^{(p+1)} - \mathbf{a}^{(p)}| / \mathbf{a}^{(p+1)}$) are both set to $1e-4$, where p is the iteration number. Practically feasible steel sections are specified after convergence by mapping the obtained continuous-valued cross-sectional properties of different member groups (defined in Fig. 3(a)) onto the corresponding catalogues of commercially available hot-finished sections. For demonstration, the mapping operation for $v_b = 30.0$ m/s is graphically demonstrated in Fig. 5(b), (c), (d), and (e) for corner posts, floor beams, ceiling beams, and bracings, respectively. In these plots, each coloured data point represents a unique hot-finished section, whose cross-sectional area, A , and second moment of inertia, I , (or the major second moment of inertia, I_y , for RHS) are given as

horizontal and vertical coordinates, respectively, whereas the obtained optimal sectional properties are denoted by black markers. In this setting, for corner posts (groups 1 to 5) and modular beams (groups 6 to 15) (for each design group) whose I or I_y is not smaller than the optimal value; for bracing members (groups 16 to 20), the mapping operation considers the cross-sectional area only. To this end, the selected steel sections for satisfying the floor acceleration constraints in Eq. (18) for three basic wind speeds are summarised in Table 2, which correspond to the discrete sizing designs represented by the unfilled triangular, square, and circular markers in Fig. 5(a). The cross-sectional areas of these three sizing designs are collected in $\mathbf{a}_{SLS}^{discrete}$ (see Fig. 2). Notably, for corner posts only, one additional buildability constraint is introduced when selecting commercially available sections, which makes sure that all posts share the same outer dimension along the building height. This consideration stems from the fact that changing the corner post size along the building height can, arguably, make the connection between adjacent modules more difficult [56].

The wind drift and inter-storey drift ratios of the optimally sized case-study building under the wind speed of 30.0 m/s are plotted in Fig. 6(a) and (b), respectively, together with the corresponding drift limits. The structural self-weight of the resized building increases slightly to 289.0 t from that of the initial design, i.e., 280.3 t, which is only designed against gravitational loads. In addition, the wind-borne RMS floor accelerations of the optimally sized case-study building for the comfort stipulation under three different wind speeds are plotted in Fig. 7, together with the corresponding ISO6897 comfort thresholds [38]. Notably, as v_b increases, the latter threshold becomes increasingly stringent because the resized building for an increased wind speed is stiffer and thus has a higher fundamental frequency. In terms of compliance, Figs. 6 and 7 show that the code-prescribed drift and floor acceleration limits are satisfied on all occupied floors of the optimal sizing designs $\mathbf{a}_{SLS}^{discrete}$. However, this is achieved at the expense of increased structural steel consumption. Specifically, for $v_b = 25.0, 27.5,$ and 30.0 m/s, the required steel tonnages of the discrete optimal sizing designs are found to be 485.2 t, 683.3 t, and 1078.8 t, respectively, which correspond to 73.1% , 143.8% , and 284.9% increments in the structural self-weight compared to the initial design reported in Fig. 3

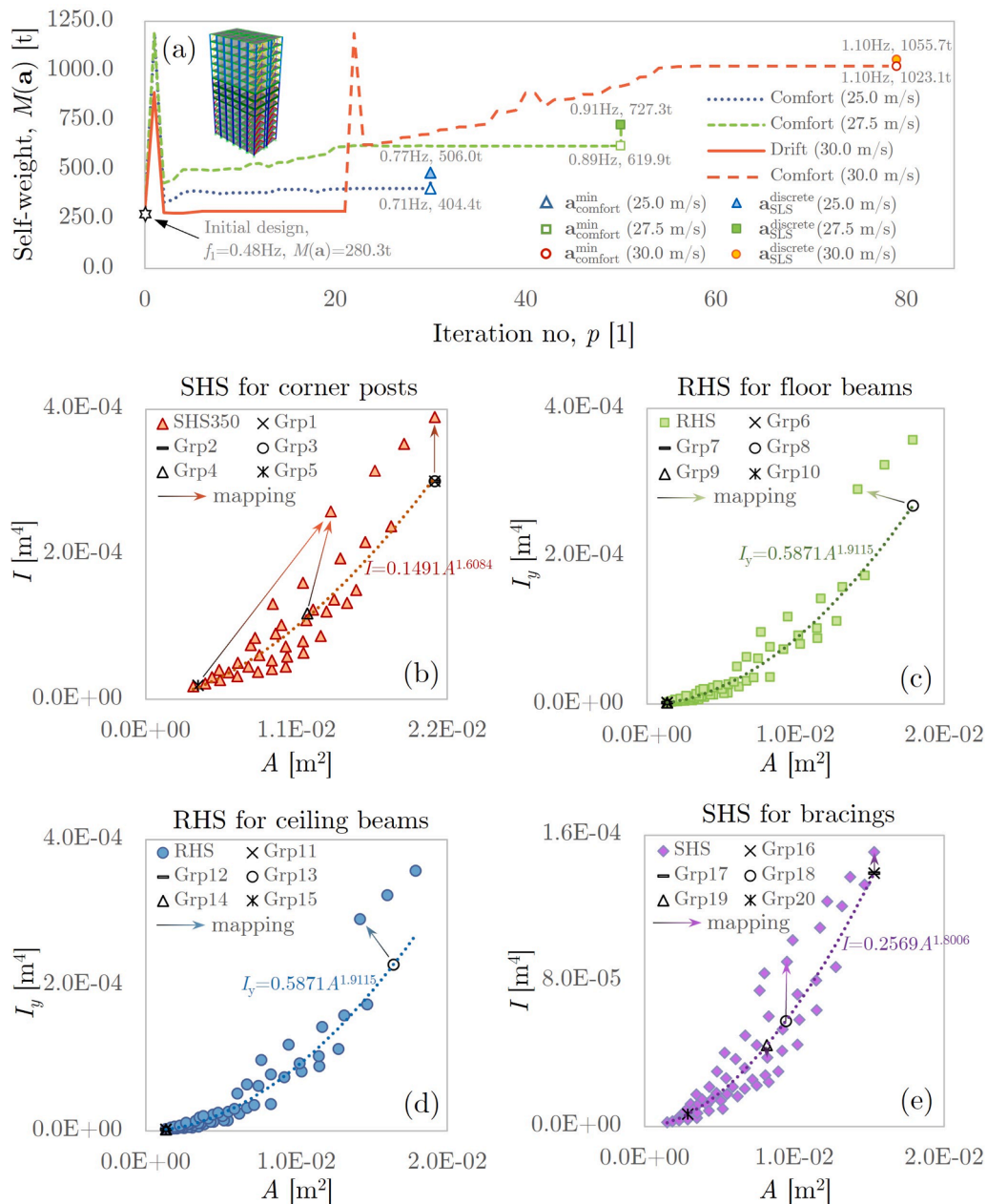


Fig. 5. (a) Sizing iterations of the case-study building under drift and floor acceleration constraints for basic wind speeds 25.0, 27.5, and 30.0 m/s, and mapping operation of continuous optimal cross-sectional properties onto different types of hot-finished steel sections for (b) corner posts, (c) floor beams, (d) ceiling beams, and (e) bracing members.

(b). Collectively, the above results suggest that typical tall self-standing MBSs can be governed by wind habitability/comfort requirements even under moderate wind excitation, whereas the wind drift limits only affect their (structural) sizing design under high wind speeds.

To shed light on the relative importance of different member groups (see Fig. 3(a)) in contributing to the lateral stiffness of the adopted building, the cross-sectional areas and major second moments of inertia of the three continuous optimal sizing designs (shown as the unfilled triangular, square, and circular markers in Fig. 5 (a)) are plotted in Fig. 8 (a) and (b), separately. As seen, for three wind speeds considered, the continuous sizing algorithm (see Section 4.1) distributes most of the structural steel to the corner posts and then bracings, with their cross-sectional areas and major second moment of inertia decreasing gradually with floor height and increasing monotonically with the wind speed. For floor and ceiling beams, however, their cross-sectional areas are

retained at the corresponding lower bounds, i.e., $\mathbf{a}_{\text{grav}}^{\text{min}}$, except for member groups 9 and 14 under $v_b = 27.5$ m/s (corresponding to modular beams in stories 7, 8, and 9) and groups 8 and 13 under $v_b = 30.0$ m/s (corresponding to modular beams in stories 10, 11, and 12). This finding suggests that the lateral stiffness of braced tall self-standing MBSs is mostly contributed by corner posts and bracings but not by modular beams. However, when the focal point of the design optimisation moves from serviceability to structural integrity, those modular beams, which are not stiffened during the SLS stage of the resizing workflow (see Fig. 2), are inadequate for passing the member strength verification under wind-related ULS load combinations. In the next section, modular beams are subjected to discrete sizing optimisation under strength constraints using the GA-based sizing algorithm described in Section 4.2.

Table 2
Optimised steel sections for the case-study building in Fig. 3(a) to satisfy drift and acceleration constraints under three different wind intensities.

Basic wind speed [m/s]	Floor	Corner posts	Floor beams	Ceiling beams	Bracings
25.0	1 – 3	SHS300/14.2	RHS120 × 60/4.0	RHS120 × 60/4.0	SHS160/6.3
	4 – 6	SHS300/10.0			
	7 – 9	SHS300/8.0			SHS160/5.0
	10 – 12				SHS120/5.0
	13–15				SHS100/4.0
27.5	1 – 3	SHS350/16.0	RHS120 × 60/4.0	RHS120 × 60/4.0	SHS180/12.5
	4 – 6				SHS250/8.0
	7 – 9	SHS350/10.0			SHS180/10.0
	10 – 12		RHS180 × 100/5.0	RHS160 × 80/5.0	SHS140/8.0
	13–15		RHS120 × 60/4.0	RHS120 × 60/4.0	SHS100/5.0
30.0	1 – 3	SHS350/16.0	RHS120 × 60/4.0	RHS120 × 60/4.0	SHS260/16.0
	4 – 6		RHS400 × 200/12.5	RHS400 × 200/12.5	SHS 250/10.0
	7 – 9	SHS350/10.0	RHS120 × 60/4.0	RHS120 × 60/4.0	SHS 180/12.5
	10 – 12				SHS 150/5.0
	13–15				

5.3. Sizing optimisation under member utilisation constraints

For modular frame members under combined axial compression and biaxial bending, they must satisfy the following buckling resistance requirements according to Eurocode 3 [30]

$$\frac{N_{Ed}}{\chi_y N_{Rk}/\gamma_{M1}} + k_{yy} \frac{M_{y,Ed}}{\chi_{LT} M_{y,Rk}/\gamma_{M1}} + k_{yz} \frac{M_{z,Ed}}{M_{z,Rk}/\gamma_{M1}} \leq 1 \text{ and} \tag{19}$$

$$\frac{N_{Ed}}{\chi_z N_{Rk}/\gamma_{M1}} + k_{zy} \frac{M_{y,Ed}}{\chi_{LT} M_{y,Rk}/\gamma_{M1}} + k_{zz} \frac{M_{z,Ed}}{M_{z,Rk}/\gamma_{M1}} \leq 1,$$

where N_{Ed} , $M_{y,Ed}$, and $M_{z,Ed}$ are the design values of the compression force and maximum moments about the y-y and z-z axes of the cross-

section based on second- or third-order analysis, respectively, χ_y , χ_z , and χ_{LT} are the reduction factors due to flexural and lateral torsional buckling, respectively, and k_{yy} , k_{yz} , k_{zy} , and k_{zz} are the interaction factors (see Section 6.3.3 of Eurocode 3 [30] for more details). In this setting, for all 20 member groups shown in Fig. 3(a), their maximum utilisation ratios calculated using the above formulas under wind-related ULS load combinations must be kept below 1.0 to avoid member overstress. However, as stated in the last section, only the modular beam groups are considered for discrete sizing optimisation under strength constraints using GA, as the utilisation ratios of corner posts and bracings of the three serviceability-compliant designs in Table 2 are found to be well below 1.0 under the corresponding levels of wind action. For demonstration, the member utilisation ratios of the serviceability-compliant design for $v_b = 30.0$ m/s are plotted in Fig. 9 (a), showing that only 8 groups of modular beams are overstressed under wind-related ULS combinations. To further facilitate the discrete sizing process, the floor and ceiling beams in the same storey are forced to use the same RHS, which halves the total number of active DVs that need to be optimised by the GA. This consideration is underpinned by the fact that the floor and ceiling beams in the same storey are found to contribute equally to the overall lateral stiffness of MBSs [57]. Moreover, it is shown later that they tend to be utilised and stressed to a similar extent under static wind loads.

To initialise the GA, the population size is set to 50 per generation, and the stopping criterion is chosen that the best penalty function value does not improve for 50 consecutive generations, or the total number of generations reaches 150. The penalty function value of a member of a population is the fitness function if the member is feasible or the maximum fitness function among feasible members of the population plus a sum of constraint violations if the member is infeasible [50]. As in Section 5.1, the sectional depth of the available RHS for modular beam groups is limited within the range of 120–400 mm to reduce the vertical spacing between the corner intra-module connections of stacked modules (see Fig. 1(c)). In this setting, there are 58 candidate RHS (as visualised in Fig. 5 (c) and (d)) available for member strength-constrained discrete sizing optimisation. At this juncture, it is worth noting that although the total number of DVs has been reduced considerably from 20 to 5 (by deactivating the member groups that do not violate the strength constraint and by requiring the ceiling and floor beams in the same storey to use the same section), discrete sizing optimisation under member strength constraints using GA is still computationally expensive, as large displacement analysis of laterally flexible building structures (such as tall self-standing MBSs with hinged IMCs) is

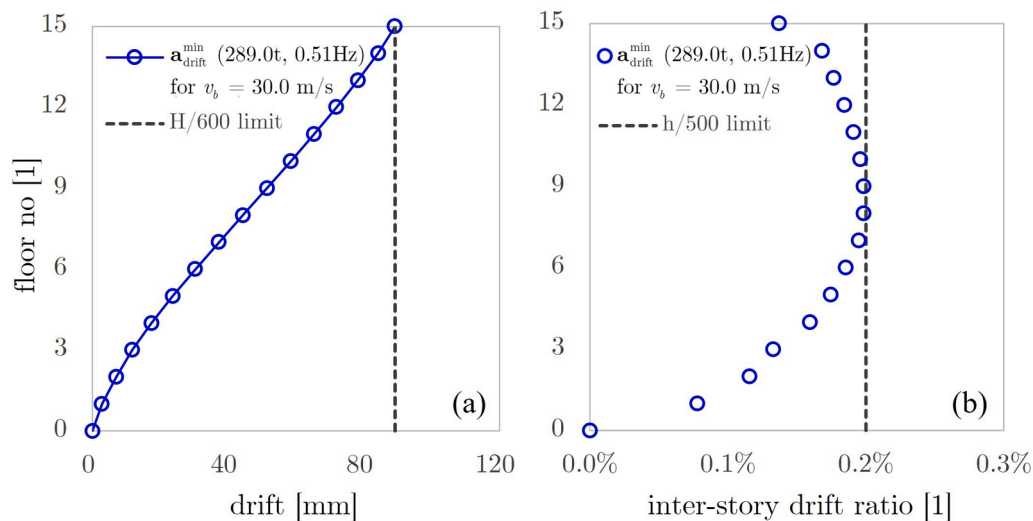


Fig. 6. Static along-wind load-induced (a) drifts and (b) inter-storey drift ratios of the optimally sized case-study building for displacement and drift ratio constraints under basic wind speed 30.0 m/s.

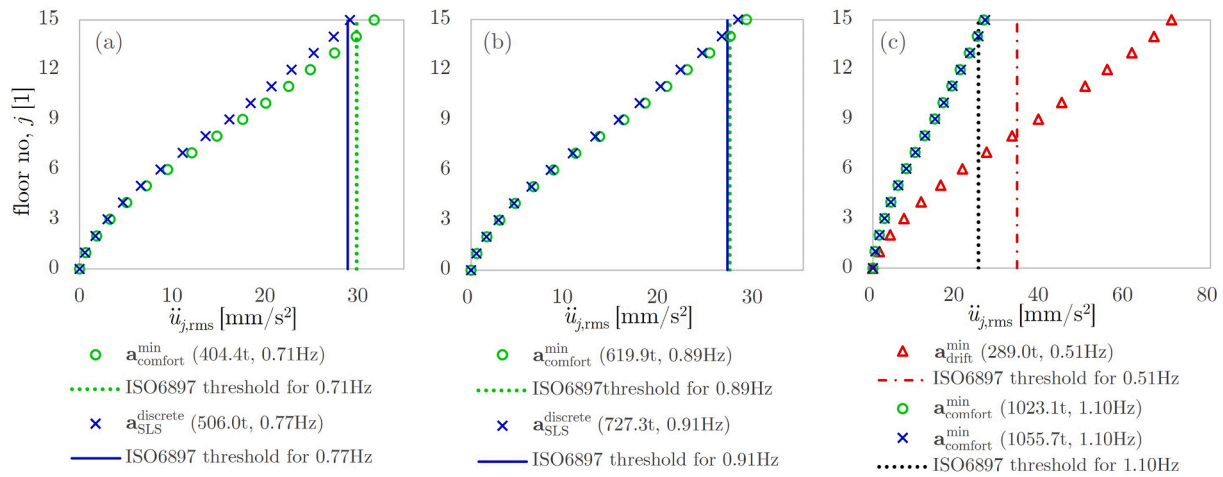


Fig. 7. Cross wind-induced RMS floor accelerations of continuous and discrete optimal sizing designs of the case-study building for basic wind speeds (a) 25.0, (b) 27.5, and (c) 30.0 m/s with ISO6897 occupant comfort thresholds.

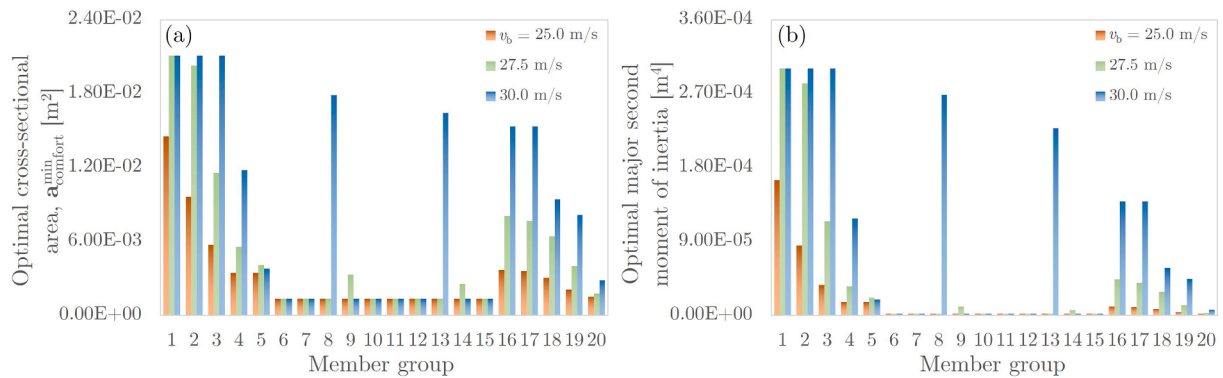


Fig. 8. Cross-sectional areas and second moments of inertia (about major bending axis) of three continuous optimal sizing designs of the case-study building in Fig. 3 (a) to satisfy drift and acceleration constraints under three different levels of static along-wind loads in Fig. 3(d) and across-wind excitations in Fig. 3(e).

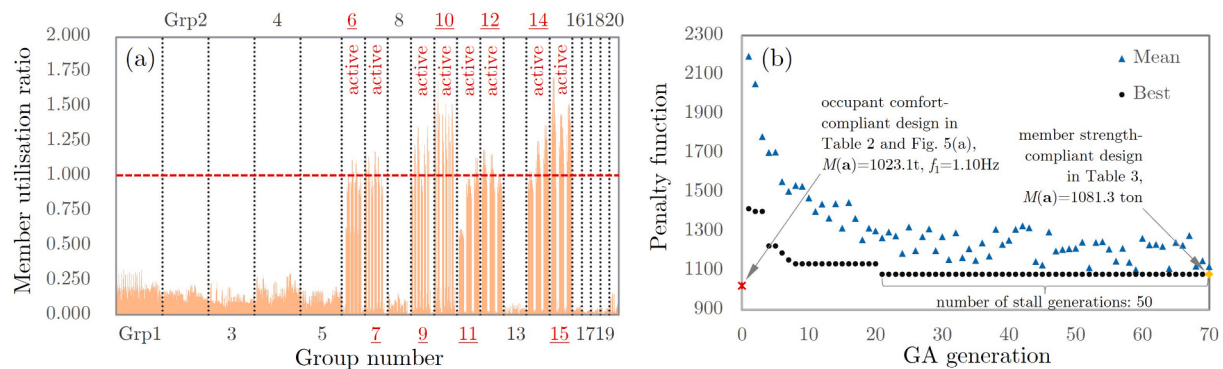


Fig. 9. (a) utilisation ratios of modular members of the comfort-optimal sizing design, $a_{comfort}^{min}$, under wind-related ultimate limit state load combinations, and (b) variation of the penalty function throughout the discrete sizing process using GA under member strength constraints for basic wind speed of 30.0 m/s.

time-consuming. Accordingly, the maximum number of iterations and the number of stall generations (whose best fitness value does not improve) are set to relatively low values.

For demonstration, the discrete sizing process under member strength constraints for $v_b = 30$ m/s using GA is plotted in Fig. 9 (b), which starts with the serviceability-compliant design (in Table 2 and Fig. 5(a)) at a self-weight of 1023.1 tons and converges after 70 generations at 1081.3 tons. As shown, the best penalty function value no longer improves after the first 21 generations, and the sizing “evolution”

is terminated after 50 stall generations at step 70. In total, 3,500 potential sizing designs are evaluated using SAP2000’s large-displacement solver, and the total core hours required to arrive at the final sizing design on a Xeon E5-1660 V4 processor (base frequency 3.20 GHz) is 99.8 h. However, it is important to note that although all genetic operations on the individual members of a generation (see Section 4.2) are sequential, the constraint function evaluation (involving large-displacement analysis and Eurocode 3-prescribed structural member verification) for different individual designs within a generation can

occur in a parallel fashion, which is the most time-consuming part of the discrete sizing process. The above discrete optimisation is also performed on the other two serviceability-compliant designs in Table 2 for their corresponding wind speeds. The optimal cross-sections of the three final sizing designs satisfying the strength constraints are detailed in Table 3. Finally, the member utilisation ratios of these three designs are plotted in Fig. 10. By cross-comparing Fig. 10 (c) and Fig. 9 (a), it is seen that by changing the cross-sections of modular beams in Table 2 to those in Table 3 for $v_b = 30.0$ m/s (with the structural self-weight increasing from 1055.7 tons to 1081.3 tons), the utilisation ratios of modular beam groups are all reduced to below 1.0. Therefore, the three designs in Table 3 are code-compliant not only in terms of the (static and dynamic) serviceability requirements but also in terms of member strength requirements. Fig. 10 shows a large variation in utilisation ratio among different member groups under wind-related ULS load combinations, regardless of wind speed. Corner posts and bracings exhibit relatively low utilisation ratios, reflecting their governance by global static and dynamic serviceability constraints. In contrast, modular beams display higher utilisation ratios due to their criticality to strength criteria. This disparity arises because tall building design under wind loads is primarily governed by lateral stiffness-related serviceability issues. As a result, most structural members of wind-sensitive tall buildings tend to fall short of full utilisation in terms of member resistance [58].

In the next section, a comprehensive performance assessment is performed on these optimal designs, shedding light on the structural behaviours of optimised tall self-standing MBSs under static and dynamic wind effects.

6. Performance assessment of optimally designed case-study building

6.1. Elastic instability based on undeformed geometries

For tall self-standing MBSs with IMCs in Fig. 1(c) and hot-finished hollow sections, the lack of column continuity (in terms of rotational stiffness) makes their structural stability under combined gravitational

Table 3

Optimal sections for the case-study building in Fig. 3(a) to satisfy member strength requirements under three different wind intensities.

Basic wind speed [m/s]	Floor	Corner posts	Floor beams	Ceiling beams	Bracings
25.0	1–3	SHS300/ 14.2	RHS140 × 80/4.0		SHS160/ 6.3
	4–6	SHS300/ 10.0			
	7–9	SHS300/ 8.0			
	10–12				
	13–15				
27.5	1–3	SHS350/ 16.0	RHS140 × 80/4.0		SHS180/ 12.5
	4–6				
	7–9	SHS350/ 10.0			
	10–12				
	13–15				
30.0	1–3	SHS350/ 16.0	RHS140 × 80/4.0		SHS260/ 16.0
	4–6				
	7–9				
	10–12	SHS350/ 10.0			
	13–15				

and lateral wind loads more difficult to predict compared to conventional building structural systems [46]. Therefore, it is deemed important to investigate the theoretical buckling strength of these structures under different wind intensities by utilising the optimally sized case-study building in Section 5.3 as a typical representation of tall self-standing MBSs. To this end, eigenvalue buckling analysis is performed on the three optimal sizing designs in Table 3 under wind related ULS load combinations in Table 1 in line with Eurocode 1 [55]. For all three buckling analyses, the first 20 buckling modes are investigated, with the eigenvalue convergence tolerance set to 1E-09. All modular members are meshed into four segments of equal length as further discretisation no longer affects the buckling analysis results.

In this setting, the first buckling modes of the three optimal sizing designs in Table 3 are obtained using the unstressed stiffness matrix and shown in the left column of Table 4, together with the buckling load factor (BLF) and buckling load case (BLC). As seen, the critical buckling modes are all associated with the bracing members in the top storey, with the BLFs equal to 2.68, 2.86, and 9.50 for basic wind speeds of 25.0, 27.5, and 30.0 m/s, respectively. Moreover, the first 20 buckling modes of the three optimal designs are all affiliated with the bracing members in the upper part of the structure, while no global buckling mode can be found within the first 20 modes. To further examine the theoretical buckling strength, the above analysis is repeated for the same optimal sizing designs and wind actions but now without discretising/meshing the bracing members. This manipulation is used to suppress the buckling modes associated with the bracing elements, allowing the retrieval of other/higher instability modes. The re-calculated buckling modes for three wind speeds are listed in the right column of Table 4. For $v_b = 25.0$ m/s, the columns of the two corner modules in storey 4 on the leeward side of the building are seen to buckle in a bow shape within the global xz plane (see Fig. 3(a)) under the ULS combination of 1.35G + 1.05Q ± 1.5Wy at the BLF of 22.48. For $v_b = 27.5$ and 30.0 m/s, the critical buckling modes are both associated with the floor and ceiling beams of modules (within the yz plane) on the ground floor. Again, no global buckling mode is observed within the first 20 eigenmodes. Collectively, these results indicate that the critical BLF of the first global instability mode is well above 10 for the three sizing designs. The latter value is a critical threshold recommended by Eurocode 3 [30] for justifying the use of first-order structural analysis to determine member design forces. However, as demonstrated in the following section, the increase in wind-induced member forces caused by the geometric nonlinearity of the structure is significant and must be accounted for in the analysis by considering third order/large-displacement effects. In this context, Section 5.2.1 of Eurocode 3 [30] may be unconservative and should be consulted with caution when designing tall self-standing MBSs.

6.2. Effects of geometric nonlinearity on wind-induced structural response and member utilisation ratios

This section aims to investigate the sensitivity of the optimal sizing designs in Table 3 to geometric nonlinear effects in terms of structural response and member design forces under wind-related SLS and ULS load combinations defined in Table 1. To this aim, the attention is first placed on wind-induced roof drift in the along-wind direction and VS-induced floor acceleration in the across-wind direction. Specifically, the static displacement response of the optimal sizing designs is assessed for three different basic wind speeds (i.e., $v_b = 25.0$, 27.5, and 30.0 m/s) using static P-Δ and large-displacement analyses, separately. The RMS floor acceleration is assessed using the standard linear frequency-domain analysis of random vibrations [59–61], with the P-Δ and large-displacement effects incorporated in the stiffness matrix. The latter is achieved conveniently by considering the geometric nonlinear effects on the case-study building under the set of factored gravitational loads, i.e., 1.0G + 0.7Q, and then using the “softened” stiffness matrix developed from this load case for the linear frequency-domain analysis under the across-wind excitation in Fig. 4(b). In general, this technique is

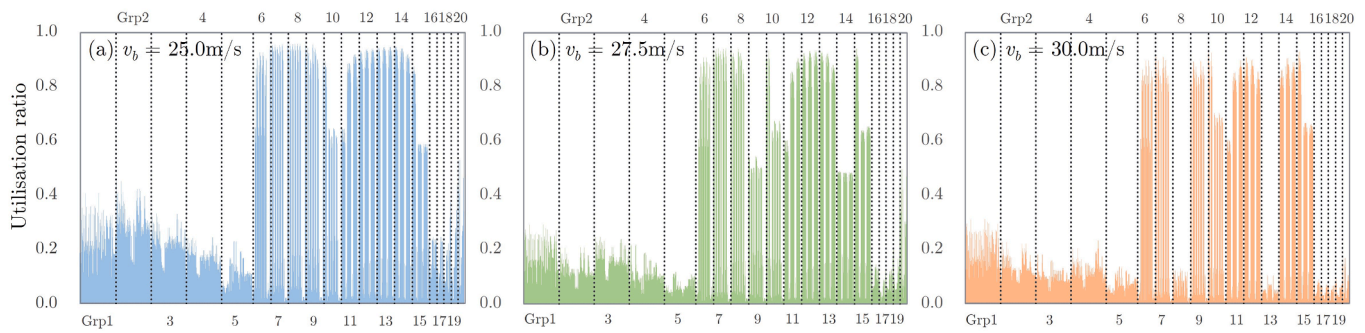
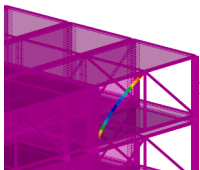
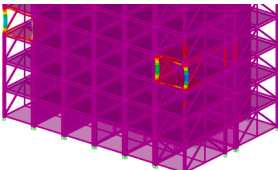
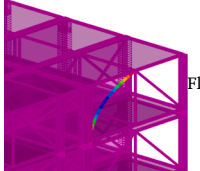
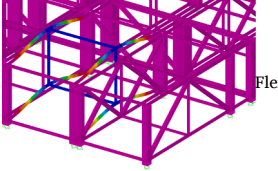
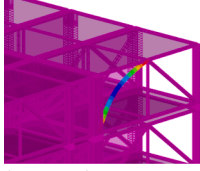
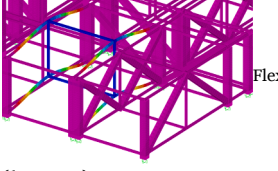


Fig. 10. Utilisation ratios of modular members of the optimal sizing designs (satisfying all design constraints) in Table 3 under wind-related ultimate limit state load combinations for basic wind speeds (a) 25.0 m/s, (b) 27.5 m/s, and (c) 30.0 m/s.

Table 4

Critical eigenvalue buckling modes of the optimal sizing designs in Table 3 under wind-related ultimate limit state load combinations for basic wind speeds 25.0, 27.5, and 30.0 m/s.

Basic wind speed [m/s]	Critical buckling mode	
	All elements meshed into 4 segments	Without meshing bracing elements
25.0	 <p>Flexural buckling of bracing (top storey) BLF: 2.68 BLC: $1.35G + 1.5Q \pm 0.9W_y$</p>	 <p>Flexural buckling of corner posts (4th storey) BLF: 22.48 BLC: $1.35G + 1.05Q \pm 1.5W_y$</p>
27.5	 <p>Flexural buckling of bracing (top storey) BLF: 2.86 BLC: $1.35G + 1.5Q \pm 0.9W_y$</p>	 <p>Flexural buckling of modular beams (1st storey) BLF: 24.42 BLC: $1.35G + 1.5Q \pm 0.9W_y$</p>
30.0	 <p>Flexural buckling of bracing (top storey) BLF: 9.50 BLC: $1.35G + 1.5Q \pm 0.9W_y$</p>	 <p>Flexural buckling of modular beams (1st storey) BLF: 17.61 BLC: $1.35G + 1.5Q \pm 0.9W_y$</p>

adequately accurate for modelling the geometric nonlinear effects due to the sway of building structures, while enabling rapid frequency-domain analysis for the purpose of design [62]. This is because the summed geometric stiffness terms of columns associated with the lateral loads is zero, and only the axial forces caused by the weight of the structure need to be included in the evaluation of the geometric stiffness terms for the complete building [63]. Finally, the accuracy of all P-Δ and large-displacement analyses are checked by re-running the analysis using a smaller step size and convergence tolerance. The roof displacement and RMS acceleration on floor 14 (the last occupied floor), normalised by the corresponding values obtained using linear/first-order static and dynamic analyses, are plotted in Fig. 11(a) and (b), respectively. For all wind speeds considered, it is seen that the roof displacements and floor acceleration predicted by P-Δ and large-displacement analyses are only slightly larger than those predicted by the first-order analysis. Also,

there is a consistent trend that the structural responses predicted by large displacement solver are always marginally larger than those by P-Δ method, and the geometric nonlinear effects on wind-induced displacement is larger than on floor acceleration. The above findings confirm that the optimal sizing designs in Table 3 obtained using the proposed sizing workflow have well-conditioned floor-by-floor stiffness-over-weight ratios, as the increase in displacements and floor accelerations are insignificant and less than 2% in general.

Next, the geometric nonlinear effects on member design forces are numerically quantified by cross-comparing member utilisation ratios obtained by linear, P-Δ, and large-displacement solvers of SAP2000 under two wind-related ULS load combinations, $1.35G + 1.5Q \pm 0.9W_y$ and $1.35G + 1.05Q \pm 1.5W_y$. The mean and peak utilisation ratios for 20 groups of modular members (see Fig. 3(a)), evaluated using Eq. (19) based on the internal forces calculated using P-Δ and large-displacement

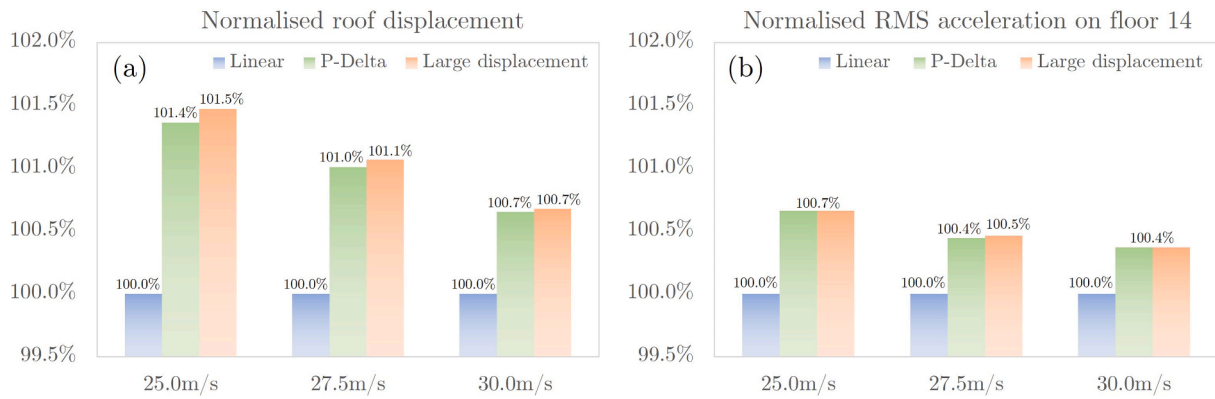


Fig. 11. (a) static along-wind load-induced roof displacements, and (b) dynamic across-wind load-induced floor acceleration on floor 14 of the optimal sizing designs in Table 3 (satisfying all SLS and ULS design constraints) predicted by P-Δ and large displacement solvers, values normalized by the corresponding values predicted by linear solver.

analyses, are normalised by the corresponding values from the linear analyses and plotted in the upper and lower rows of Fig. 12, respectively. As shown, using P-Δ solver does not lead to significant increase in the member design forces, as both normalised mean and peak utilisation ratios for all member groups and wind intensities are only slightly above 100%. However, member design forces are “amplified” significantly by large-displacement analysis, which tracks the positions/orientations of structural elements under the external loads using an updated Lagrangian formulation and considers the equilibrium equations in the deformed configuration of the structure [64]. For the adopted modular building, the increase in the peak utilisation ratios for corner posts in the upper stories and floor beams can be as excessive as 400%. The above observation suggests that the effects of large displacements and rotations upon the modular members of tall self-standing buildings must be considered properly in the analysis. Failure to do so may significantly underestimate the internal forces for member design, potentially causing even more excessive geometric nonlinear effects and member

overstress.

6.3. Effects of global sway imperfections on member utilisation ratios

In this section, the effects of global geometric imperfections on the wind-induced member forces of the optimally designed case study building are assessed for the three wind speeds considered before. For the adopted building, it is numerically verified that the lateral static wind loads are less than 15% of the gravity loads at all floors. Accordingly, the global imperfections need to be considered for wind-related load combinations according to Eurocode 3 [30]. These imperfections can be due to a lack of verticality/straightness of structural members, lack of mechanical fit, and minor eccentricities in the IMCs of modular buildings. As in Section 6.2, member imperfections are not allowed in the structural analysis but accounted for when determining member resistances, which is the standard European and UK practice [65]. According to Eurocode 3 [30], the assumed shape of global imperfections

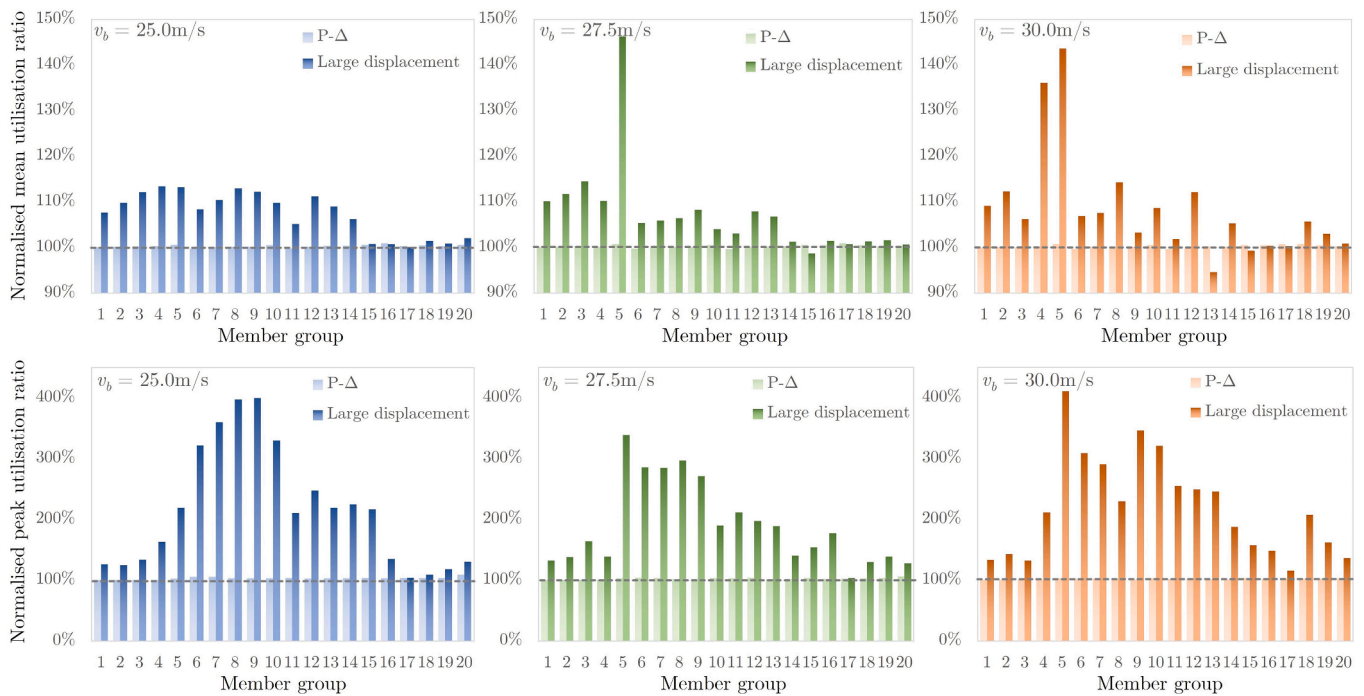


Fig. 12. Mean (upper row) and peak (lower row) utilisation ratios of modular member groups of the optimal sizing designs in Table 3 evaluated by P-Δ and large displacement solvers for basic wind speeds 25.0 m/s (left column), 27.5 m/s (middle column), and 30.0 m/s (right column), values normalized by the corresponding utilisation ratios evaluated by linear solver.

may be derived from the global elastic buckling mode of the structure in the buckling plane considered. However, this is not easy to implement for the adopted building, as its global sway (buckling) modes cannot be identified for the three optimal designs in Table 3 under the two wind-related ULS load combinations in Table 1. To this end, the first translational vibration modes of the three sizing designs in Table 3 (all in the y-z plane) are adopted separately as the initial global imperfections, with the imperfection amplitudes at the roof level all set to $H/300$ following the recommendations by Eurocode 3 [30]. This allowance takes into the basic value for global out-of-verticality imperfection and the reduction factor for building height H (see Eurocode 3 [30]). Notably, the above imperfection amplitude is larger than the normally specified tolerances for tall MBSs [12], and thus conservative for the purpose at hand. At this juncture, structural analysis of the three optimal designs in Table 3 under the two wind-related ULS combinations with and without the above global imperfections is performed using the large-displacement solver of SAP2000, as it is established in Section 6.2 that the effects of deformed positions/orientations of modular members on member forces are significant under combined gravitational and wind loads. The averaged and peak member utilisation ratios of the three sizing designs with global imperfections are normalised by the corresponding values of the same designs without imperfections and plotted in Fig. 13 for all 20 (member) design groups (defined in Fig. 3 (a)) and for three basic wind speeds.

As shown in Fig. 13 (a), the normalised mean utilisation ratios of corner posts, floor beams, and ceiling beams are not significantly affected by the global sway imperfections, as the differences in the ratios are found to be less than 1% across all wind speeds considered. For bracing members, the increases are slightly higher but still within 5%. Nevertheless, as shown in Fig. 13 (b), the increase in the peak utilisation ratios due to the sway imperfections are much larger, especially for modular beams and bracing members. Specifically, for corner posts, floor beams, ceiling beams, and bracings, the maximum increases in the peak utilisation ratios across the three wind speeds are 9.1%, 26.6%, 36.3%, and 37.2%, respectively. This finding suggests that tall self-standing MBSs, even after optimal sizing for serviceability and strength requirements, can be still sensitive to global sway imperfections, which must be considered properly in structural analysis such that its amplification effects on member design forces/moments are not underestimated in design. Nevertheless, it is important to note that the building quality of prefabricated modular units is closely monitored and controlled in a factory environment through precision manufacturing, and a high level of precision can be achieved at construction sites by practicing accurate assembly techniques. Accordingly, the global sway imperfections in realistic tall modular buildings may be much smaller than the assumed value of $1/300H$.

7. Summary and concluding remarks

In this study, a performance-based sizing optimisation framework was developed to reduce the structural self-weight of wind-sensitive tall self-standing modular buildings subjected to multiple performance constraints. This was achieved by formulating a constrained sizing optimisation problem for tall modular buildings to meet the along-wind drift and across-wind occupant comfort criteria, which govern the global structural design in the serviceability limit state (SLS), and to satisfy member strength requirements, which govern the member design in the ultimate limit state (ULS). An efficient numerical solution strategy was devised to solve the constrained discrete weight minimisation problem by first reformulating the drift and acceleration criteria as a structural compliance and natural frequency constraints, separately, and then by decoupling the original optimisation problem into two sequential stages: a convex SLS stage and nonconvex ULS stage. The latter can be solved using any combination of local and global optimisation methods, respectively. For numerical application of the framework, an interior point method was used for minimal sizing under either a structural compliance or natural frequency constraint, whereas a genetic algorithm was used for minimal sizing under member strength constraints while accounting for geometric nonlinear effects. The applicability of the proposed sizing framework was demonstrated using a 15-storey self-standing modular building exposed to three different basic wind speeds ranging from 25.0 to 30.0 m/s. The adopted building has a very common structural configuration and module arrangement, which arguably makes it a representative benchmark structure for studying the structural behaviours of tall self-standing modular buildings under different wind conditions. For each wind velocity, the optimal discrete sizing designs satisfying the drift, floor acceleration, and member strength constraints were obtained using a structural optimisation application developed using SAP2000's Open Application Programming Interface, which allows for the integration of SAP2000 (for structural analysis) and MATLAB (for constrained optimisation). The structural performance of the three optimal designs under combined gravitational and wind loads was comprehensively assessed in line with Eurocode 3 [30]. Insights were provided into the case-study building's elastic instability behaviour, geometric nonlinear effects on wind-induced responses, and impacts of global sway imperfections on member design forces, with the main findings summarised as follows.

1. By comparing the sectional properties of different member groups of the three optimal designs, it was found that increasing the size of corner posts and bracings was more effective in enhancing the lateral stiffness of the case-study building than enlarging the ceiling and floor beams. This observation emphasises the relative importance of corner posts and bracings in the static and dynamic serviceability

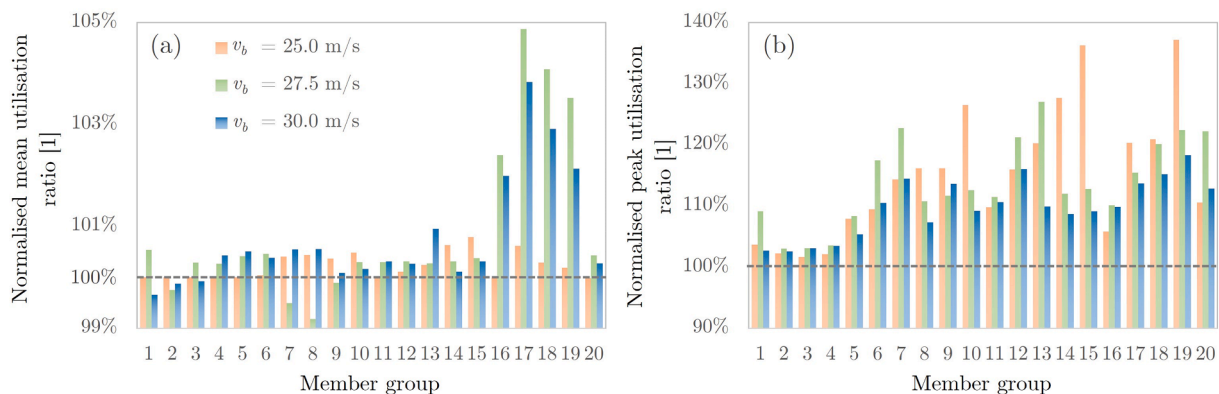


Fig. 13. (a) average and (b) peak normalised utilisation ratios of modular member groups of the optimal sizing designs in Table 3 (satisfying all SLS and ULS design constraints) with global sway imperfections evaluated using large displacement solvers, values normalised by the corresponding values of the same optimal designs without imperfections.

- design of tall self-standing MBSs with similar structural layouts to that of the case-study building.
- For the three wind speeds considered, it was found that the serviceability design of the case-study building was governed by the across-wind floor acceleration constraints but not by the along-wind drift requirements. In this regard, inter-module connections (IMCs) may play a critical role in affecting the dynamic acceleration response of tall self-standing MBSs under wind excitations; these bolted joints can offer additional energy dissipation to the building through friction and material damping when, for instance, high damping material(s) is used. Alternatively, supplementary damping devices [60,61,66,67,68] can be utilised to enhance the habitability of tall self-standing modular buildings under wind excitations. This, in turn, reduces the amount of structural material needed to increase the lateral stiffness of the building (see [19]). Furthermore, at the member level, the size of corner posts and bracings of the case-study building was governed by overall dynamic stiffness requirements to satisfy the comfort stipulation, whereas modular beams were governed by strength criteria to satisfy the buckling resistance requirement.
 - Regarding the elastic buckling behaviour, the optimal sizing designs of the case-study building with hinged IMCs demonstrated no global buckling modes under wind-related ULS load combinations for all wind intensities considered. This finding suggests that the resilience of tall self-standing MBSs against global instability under combined gravitational and high winds (e.g., $v_b = 30.0$ m/s) may be achieved by structural sizing for serviceability and integrity requirements. More importantly, the critical elastic buckling factor of 10.0 by Eurocode 3 [30], which may be used to justify the first-order structural analysis when satisfied, was found unconservative for the case-study building. This finding warrants further research to determine a more appropriate value for tall self-standing MBSs.
 - In terms of geometric nonlinearity, its effects on amplifying the wind-induced (static) displacement and acceleration responses of the optimally sized case-study building were insignificant. Therefore, the global SLS design of tall self-standing MBSs, with similar structural layouts to that of the case-study building, may be performed using first-order analysis. However, for structural member design, the effect of large displacements and rotations (i.e., third-order effects) on modular members must be accounted for in the analysis. Using second-order analysis may still underestimate the internal forces for member design, potentially causing even more excessive geometric nonlinear effects and member overstress.
 - It was found that global sway imperfections had significant impacts on the member utilisation ratios of the case-study building calculated using Eurocode 3 [30], particularly for the modular beams and bracing members. This finding suggests that tall self-standing MBSs may be highly sensitive to global sway imperfections, which must be adequately considered in structural analysis to avoid underestimating their amplification effects on member design forces.
 - For the basic wind speeds of 25.0, 27.5, and 30.0 m/s, the corresponding optimal sizing designs of the case-study building was found to have a structural self-weight of 78.3, 112.7, and 160.6 kg/m², respectively. At the moderate wind speed of 25.0 m/s, the self-weight of the optimal sizing design was comparable to the average weight of steel frameworks for typical 10- to 15-storey high-rise buildings (usually around 75 – 90 kg/m² [69]) that use conventional structural systems.

As a final remark, the current study has confirmed that tall, self-standing modular buildings are structurally feasible under high wind conditions with reasonable steel tonnages. With the proposed optimisation-driven design framework, such buildings can achieve even greater cost reduction, beyond the current rate of 10% to 20% [4] (which is based on non-optimally sized modular buildings), as well as faster construction times (as all building components can be

prefabricated offsite with no onsite construction required). From a structural optimisation standpoint, the proposed framework offers an efficient and flexible sizing approach for minimum-weight design of self-standing modular structures subjected to concurrent, wind-related serviceability and strength constraints. The proposed framework is envisioned to serve as a useful tool for creating wind-resilient and material-efficient tall self-standing modular buildings.

Declaration of Competing Interest

The authors declare that they have no known competing financial interests or personal relationships that could have appeared to influence the work reported in this paper.

Data availability

No data was used for the research described in the article.

References

- United Nations, Department of Economic and Social Affairs, Population Division. World Urbanization Prospects: The 2018 Revision. New York: United Nations; 2019.
- Farnsworth D. *Modular Tall Building Design at Atlantic Yards B2. Future Cities: Towards Sustainable Vertical Urbanism*; 2014. p. 492–9.
- Gorgolewski MT, Grubb PJ, Lawson RM. *Modular Construction using Light Steel Framing: Design of Residential Buildings*. Ascot: SCI; 2001.
- Ahn YH, Kim K-T. Sustainability in modular design and construction: a case study of 'The Stack'. *Int J Sustain Build Technol Urban Dev* 2015;5:250–9. <https://doi.org/10.1080/2093761x.2014.985758>.
- Nahmens I, Ikuma LH. Effects of Lean Construction on Sustainability of Modular Homebuilding. *J Archit Eng* 2012;18:155–63. [https://doi.org/10.1061/\(asce\)ae.1943-5568.0000054](https://doi.org/10.1061/(asce)ae.1943-5568.0000054).
- Corfar D-A, Tsavdaridis KD. A comprehensive review and classification of inter-module connections for hot-rolled steel modular building systems. *J Build Eng* 2022;50:104006. <https://doi.org/10.1016/j.jobte.2022.104006>.
- Jabar I laili, Ismail F, Mustafa AA. Issues in Managing Construction Phase of ISB Projects. *Procedia - Soc Behav Sci*. 2013;101:81–9. <https://doi.org/10.1016/j.sbspro.2013.07.181>.
- Kamali M, Hewage K. Life cycle performance of modular buildings: A critical review. *Renew Sustain Energy Rev* 2016;62:1171–83. <https://doi.org/10.1016/j.rser.2016.05.031>.
- Lawson RM, Ogden RG, Bergin R. Application of Modular Construction in High-Rise Buildings. *J Archit Eng* 2012;18:148–54. [https://doi.org/10.1061/\(asce\)ae.1943-5568.0000057](https://doi.org/10.1061/(asce)ae.1943-5568.0000057).
- Hickey J, Broderick B, Fitzgerald B, Moore H. Mitigation of wind induced accelerations in tall modular buildings. *Structures* 2022;37:576–87. <https://doi.org/10.1016/j.istruc.2022.01.037>.
- Hough MJ, Lawson RM. Design and construction of high-rise modular buildings based on recent projects. *Proc Inst Civil Eng - Civil Eng* 2019;172:37–44. <https://doi.org/10.1680/jcienv.18.00058>.
- Lawson RM, Richards J. Modular design for high-rise buildings. *Proc Inst Civil Eng - Struct Build* 2010;163:151–64. <https://doi.org/10.1680/stbu.2010.163.3.151>.
- Styles AJ, Luo FJ, Bai Y, Murray-Parke JB. Effects of joint rotational stiffness on structural responses of multi-storey modular buildings. In: Mair RJ, Soga K, Jin Y, Parlikad AK, Schooling JM, editors., ICE Publishing; 2016, p. 457–62. <https://doi.org/10.1680/tfists.161279.457>.
- Lacey AW, Chen W, Hao H, Bi K. Effect of inter-module connection stiffness on structural response of a modular steel building subjected to wind and earthquake load. *Eng Struct* 2020;213. <https://doi.org/10.1016/j.engstruct.2020.110628>.
- Chua YS, Liew JYR, Pang SD. Modelling of connections and lateral behavior of high-rise modular steel buildings. *J Constr Steel Res* 2020;166. <https://doi.org/10.1016/j.jcsr.2019.105901>.
- Elsayed M, A. Mutalib A, Elsayed K. Numerical Study of Structural Performance and Wind Flow Dynamic Behavior for PPVC Steel Modular Construction (MSC) under Various Extreme Wind Loads. *Buildings* 2022;12:1347. <https://doi.org/10.3390/buildings12091347>.
- Hildahl B. Developers | Is 2022 the year for modular? Base4 - Blog n.d. <https://www.base-4.com/developers-is-2022-the-year-for-modular/> (accessed November 29, 2022).
- Modular Building Institute. Vertical Engineering: Inside the World's Tallest Modular Building with MJH Structural Engineers' Michael Hough n.d. <https://www.modular.org/2022/09/26/vertical-engineering-inside-the-worlds-tallest-modular-building/> (accessed November 29, 2022).
- Wang Z, Giaralis A. A novel integrated optimization-driven design framework for minimum-weight lateral-load resisting systems in wind-sensitive buildings equipped with dynamic vibration absorbers. *Structural Control and Health Monitoring* n.d.
- IEA. 2019 Global Status Report for Buildings and Construction: Towards a zero-emissions, efficient and resilient buildings and construction sector. UNEP; 2019.

- [21] Robati M, Oldfield P, Nezhad AA, Carmichael DG, Kuru A. Carbon value engineering: A framework for integrating embodied carbon and cost reduction strategies in building design. *Build Environ* 2021;192:107620. <https://doi.org/10.1016/j.buildenv.2021.107620>.
- [22] Moynihan MC, Allwood JM. Utilization of structural steel in buildings. *Proc R Soc A* 2014;470:20140170. <https://doi.org/10.1098/rspa.2014.0170>.
- [23] Taranath BS. *Tall Building Design: Steel, Concrete, and Composite Systems*. Boca Raton: CRC Press; 2017.
- [24] Chan C-M, Chui JKL. Wind-induced response and serviceability design optimization of tall steel buildings. *Eng Struct* 2006;28:503–13. <https://doi.org/10.1016/j.engstruct.2005.09.005>.
- [25] Chan CM, Huang MF, Kwok KCS. Stiffness Optimization for Wind-Induced Dynamic Serviceability Design of Tall Buildings. *J Struct Eng* 2009;135:985–97. [https://doi.org/10.1061/\(ASCE\)ST.1943-541X.0000036](https://doi.org/10.1061/(ASCE)ST.1943-541X.0000036).
- [26] Fu J, Zheng Q, Huang Y, Wu J, Pi Y, Liu Q. Design optimization on high-rise buildings considering occupant comfort reliability and joint distribution of wind speed and direction. *Eng Struct* 2018;156:460–71. <https://doi.org/10.1016/j.engstruct.2017.11.041>.
- [27] Spence SMJ. Optimization of uncertain and dynamic high-rise structures for occupant comfort: An adaptive kriging approach. *Struct Saf* 2018;75:57–66. <https://doi.org/10.1016/j.strusafe.2018.05.008>.
- [28] Huang MF, Chan CM, Lou WJ. Optimal performance-based design of wind sensitive tall buildings considering uncertainties. *Comput Struct* 2012;98–99:7–16. <https://doi.org/10.1016/j.compstruc.2012.01.012>.
- [29] Kareem A, Kijewski T, Tamura Y. Mitigation of motions of tall buildings with specific examples of recent applications. *Wind Struct* 1999;2:201–51. <https://doi.org/10.12989/WAS.1999.2.3.201>.
- [30] BSI. *Eurocode 3: Design of steel structures - Part 1–1: General rules and rules for buildings*. London: BSI; 2015.
- [31] Mendis P, Ngo T, Haritos N, Hira A, Samali B, Cheung J. Wind Loading on Tall Buildings. *EJSE* 2007;41–54. <https://doi.org/10.56748/ejse.641>.
- [32] CTBUH. *CTBUH Height Criteria for Measuring & Defining Tall Buildings*. The Council on Tall Buildings and Urban Habitat; n.d.
- [33] Khodaie N. Vibration control of super-tall buildings using combination of tapering method and TMD system. *J Wind Eng Ind Aerodyn* 2020;196:104031. <https://doi.org/10.1016/j.jweia.2019.104031>.
- [34] Li QS, Xiao YQ, Wong CK, Jeary AP. Field measurements of typhoon effects on a super tall building. *Eng Struct* 2004;26:233–44. <https://doi.org/10.1016/j.engstruct.2003.09.013>.
- [35] Griffis LG. Serviceability Limit States Under Wind Load. *Eng J* 1993;16.
- [36] Simiu E, Scanlan RH. *Wind effects on structures: fundamentals and applications to design*. 3rd ed. New York: John Wiley; 1996.
- [37] Liang S, Liu S, Li QS, Zhang L, Gu M. Mathematical model of acrosswind dynamic loads on rectangular tall buildings. *J Wind Eng Ind Aerodyn* 2002;90:1757–70. [https://doi.org/10.1016/S0167-6105\(02\)00285-4](https://doi.org/10.1016/S0167-6105(02)00285-4).
- [38] ISO. Guidelines for the evaluation of the response of occupants of fixed structures, especially buildings and off-shore structures, to low-frequency horizontal motion (0.063 to 1 Hz). 1st ed. 1984.
- [39] Architectural Institute of Japan. *Guidelines for the evaluation of habitability to building vibration*. Tokyo: AIJ; 2007.
- [40] Bernardini E, Spence SMJ, Kwon D-K, Kareem A. Performance-Based Design of High-Rise Buildings for Occupant Comfort. *J Struct Eng* 2015;141:04014244. [https://doi.org/10.1061/\(ASCE\)ST.1943-541X.0001223](https://doi.org/10.1061/(ASCE)ST.1943-541X.0001223).
- [41] ASCE. *Minimum Design Loads for Buildings and Other Structures*. ASCE; 1996. <https://doi.org/10.1061/9780784400920>.
- [42] Kareem A. *Serviceability Issues and Motion Control of Tall Buildings*. San Antonio, TX: ASCE; 1992.
- [43] Burton MD, Kwok KC, Hitchcock PA, Denoon RO. Frequency Dependence of Human Response to Wind-Induced Building Motion. *J Struct Eng* 2006;132:296–303. [https://doi.org/10.1061/\(ASCE\)0733-9445\(2006\)132:2\(296\)](https://doi.org/10.1061/(ASCE)0733-9445(2006)132:2(296)).
- [44] Svanberg K. *On local and global minima in structural optimization. New directions in optimum structural design*. Chichester: Wiley; 1984.
- [45] Piotrowski AP, Napiorkowski JJ, Piotrowska AE. Population size in Particle Swarm Optimization. *Swarm Evol Comput* 2020;58:100718. <https://doi.org/10.1016/j.swevo.2020.100718>.
- [46] Farajian M, Sharafi P, Kildashti K. The influence of inter-module connections on the effective length of columns in multi-story modular steel frames. *J Constr Steel Res* 2021;177:106450. <https://doi.org/10.1016/j.jcsr.2020.106450>.
- [47] Christensen PW, Klarbring A. *An Introduction to Structural Optimization*. 1st ed. Dordrecht: Springer; 2009.
- [48] Byrd RH, Hribar ME, Nocedal J. An Interior Point Algorithm for Large-Scale Nonlinear Programming. *SIAM J Optim* 1999;9:877–900. <https://doi.org/10.1137/S1052623497325107>.
- [49] Deb K. An efficient constraint handling method for genetic algorithms. *Comput Methods Appl Mech Engrg* 2000;28.
- [50] Deep K, Singh KP, Kansal ML, Mohan C. A real coded genetic algorithm for solving integer and mixed integer optimization problems. *Appl Math Comput* 2009;212:505–18. <https://doi.org/10.1016/j.amc.2009.02.044>.
- [51] Goldberg DE, Deb K. A Comparative Analysis of Selection Schemes Used in Genetic Algorithms. In: RAWLINS GJE, editor. *Foundations of Genetic Algorithms*, vol. 1, Elsevier; 1991, p. 69–93. <https://doi.org/10.1016/B978-0-08-050684-5.50008-2>.
- [52] Li G-Q, Cao K, Lu Y, Jiang J. Effective Length Factor Of Columns In Non-Sway Modular Steel Buildings. *Adv Steel Constr* 2017;13:412–26. <https://doi.org/10.18057/ijasc.2017.13.4.6>.
- [53] Stora Enso. *3–8 Storey Modular Element Buildings* 2016.
- [54] Lawson RM, Ogden RG, Goodier C. *Design in Modular Construction*. Oxon: CRC Press; 2014.
- [55] BSI. *Eurocode 1: Actions on structures - Part 1–4: General actions - Wind actions*. London: BSI; 2011.
- [56] Thai H-T, Ngo T, Uy B. A review on modular construction for high-rise buildings. *Structures* 2020;28:1265–90. <https://doi.org/10.1016/j.istruc.2020.09.070>.
- [57] Wang Z, Tsavdaridis KD. Optimality criteria-based minimum-weight design method for modular building systems subjected to generalised stiffness constraints: A comparative study. *Eng Struct* 2022;251:113472. <https://doi.org/10.1016/j.engstruct.2021.113472>.
- [58] Chun-Man C, Grierson DE, Sherbourne AN. Automatic Optimal Design of Tall Steel Building Frameworks. *J Struct Eng* 1995;121:838–47. [https://doi.org/10.1061/\(ASCE\)0733-9445\(1995\)121:5\(838\)](https://doi.org/10.1061/(ASCE)0733-9445(1995)121:5(838)).
- [59] Soong TT, Grigoriu M. *Random Vibration of Mechanical and Structural Systems*. PTR Prentice Hall 1993.
- [60] Petrini F, Giaralis A, Wang Z. Optimal tuned mass-damper-inerter (TMDI) design in wind-excited tall buildings for occupants' comfort serviceability performance and energy harvesting. *Eng Struct* 2020;204:109904. <https://doi.org/10.1016/j.engstruct.2019.109904>.
- [61] Wang Z, Giaralis A. Top-Story Softening for Enhanced Mitigation of Vortex Shedding-Induced Vibrations in Wind-Excited Tuned Mass Damper Inerter-Equipped Tall Buildings. *J Struct Eng* 2021;147:04020283. [https://doi.org/10.1061/\(ASCE\)ST.1943-541X.0002838](https://doi.org/10.1061/(ASCE)ST.1943-541X.0002838).
- [62] Computers and Structures, Inc. *CSI Analysis Reference Manual*. Berkeley: Computers and Structures, Inc.; 2016.
- [63] Wilson EL. *Three dimensional static and dynamic analysis of structures: a physical approach with emphasis on earthquake engineering*. Berkeley: Computers and Structures; 2000.
- [64] Bathe K-J, Bolourchi S. Large displacement analysis of three-dimensional beam structures. *Int J Numer Meth Engrg* 1979;14:961–86. <https://doi.org/10.1002/nme.1620140703>.
- [65] Brettle ME, Brown DG. *Steel building design: concise Eurocodes, in accordance with Eurocodes and the UK National Annexes*. Berkshire: SCI; 2009.
- [66] Elias S, Matsagar V. Research developments in vibration control of structures using passive tuned mass dampers. *Annu Rev Control* 2017;44:129–56. <https://doi.org/10.1016/j.arcontrol.2017.09.015>.
- [67] Suthar SJ, Jangid RS. Design of tuned liquid sloshing dampers using nonlinear constraint optimization for across-wind response control of benchmark tall building. *Structures* 2021;33:2675–88. <https://doi.org/10.1016/j.istruc.2021.05.059>.
- [68] Suthar Sameer J., Patil Veeranagouda B., Jangid Radhey Shyam. Optimization of MR Dampers for Wind-Excited Benchmark Tall Building. *Practice Periodical on Structural Design and Construction* 2022;27:04022048. [https://doi.org/10.1061/\(ASCE\)SC.1943-5576.0000733](https://doi.org/10.1061/(ASCE)SC.1943-5576.0000733).
- [69] SteelConstruction.info. *Cost of structural steelwork*. SteelConstructionInfo - The Free Encyclopedia for UK Steel Construction Information n.d.